

STUDY OF HIGH-THROUGHPUT PARTICLE SEPARATION DEVICE
BASED ON STANDING SURFACE ACOUSTIC WAVE (SSAW) TECHNOLOGY

A Thesis

Presented to

The Graduate Faculty of The University of Akron

In Partial Fulfillment

of the Requirements for the Degree

Master of Science

Zhuochen Wang

August, 2012

STUDY OF HIGH-THROUGHPUT PARTICLE SEPARATION DEVICE
BASED ON STANDING SURFACE ACOUSTIC WAVE (SSAW) TECHNOLOGY

Zhuochen Wang

Thesis

Approved:

Accepted:

Advisor

Dr. Jiang J. Zhe

Department Chair

Dr. Celal Batur

Faculty Reader

Dr. Guoxiang Wang

Dean of the College

Dr. George K. Haritos

Committee Member

Dr. Jae-won Choi

Dean of the Graduate School

Dr. George R. Newkome

Date

ABSTRACT

Manipulation of microscale particles and fluid liquid droplets is an important task for lab-on-a-chip devices for numerous biological researches and applications, such as cell detection and tissue engineering. Particle manipulation techniques based on surface acoustic waves (SAW) appear effective for lab-on-a-chip devices because they are non-invasive, compatible with soft lithography micromachining, have high energy density, and can work for nearly any type of microscale particles.

In this thesis, a new two-stage particle separation device based on standing surface acoustic waves was developed. The different sizes of particles were firstly focused in a line at the first stage and then separated at the second stage. This device only utilizes standing surface acoustic force in both stages, does not require sheath flow, avoiding any risk of contamination of sample and simplifying the stature of the device.

The electrode was patterned and etched on a golden coated LiNbO_3 wafer by photolithography. The PDMS microchannel was fabricated by curing it on a mold that was fabricated on glass substrate also by photolithography. Then we bonded the electrode and PDMS channel together under a microscope with designed align marks.

The device was tested using two kinds of micro particles with different sizes, 20 μm polystyrene beads and 5 μm polystyrene beads, which were separated in a short time. Experimental conditions including applied voltage, frequency and flow velocity were optimized to increase efficiency and throughput. A high throughput of 50 $\mu\text{L}/\text{hour}$ was achieved by this device, which is a few time higher than that of existing similar micro devices (typically have a throughput less than 20 $\mu\text{L}/\text{hour}$).

A SSAW separation device with a wide separation channel was also tested to increase the throughput dramatically. The throughput of this wide channel device can reach up to 300 $\mu\text{L}/\text{hour}$. The feasibility of separating blood was studied and confirmed by calculation as well.

ACKNOWLEDGEMENTS

During this research, I have worked with so many people whose contribution to the research deserves a special mention. The work presented here would not have been completed without their kindly help.

A special word of thanks is due to my adviser, Dr. Jiang Zhe, who has led me into the wonderful field of MEMS, which I knew little about it before. Dr Jiang Zhe has guided, inspired and motivated me and has given me the invaluable help during my study and research work in these two years. I would like to express my indebtedness to Dr. Guoxiang Wang and Dr. Jae-won Choi who have made valuable suggestions, specialist advices and critical comments on the thesis. I would like to thank my colleagues, Mr. Li Du, Dr. Ashish Jagtiani, Mr. Yu Han, Mr. Abdullah Amin and Mr. Akram Hossein for their help and support during this research and my Master's course.

Finally, I am forever thankful to My Parents and My fiancée for their support, constant encouragement and everlasting love.

TABLE OF CONTENTS

	Page
LIST OF FIGURES.....	ix
LIST OF TABELS.....	xv
CHAPTER	
I. INTRODUCTION.....	1
1.1 Introduction.....	1
1.2 Motivation.....	3
1.3 Objective.....	3
1.4 Significance of Study.....	4
1.5 Specific Goals.....	5
1.6 Outline.....	6
II. BACKGROUND AND LITERATURE REVIEW.....	7
2.1 Introduction of SAW.....	7
2.2 Application of SAW.....	8
2.2.1 Particle focusing and separating.....	9
2.2.2 Particle alignment and patterning.....	14
2.2.3 Particle directing.....	20
2.2.4 Liquid droplet delivery.....	24
III. DESIGN AND CALCULATION.....	30
3.1 Theory analysis.....	30

3.2 Design plans.....	37
3.2.1 Option one.....	37
3.2.2 Option two.....	38
3.2.3 Option three.....	40
3.3 Calculation.....	41
3.4 Design of IDTs.....	46
3.5 Design of channel.....	47
3.6 Select of substrate.....	47
IV. FABRICATION.....	49
4.1 Electrode fabrication.....	49
4.2 Channel fabrication.....	52
4.2.1 Mold fabrication.....	52
4.2.2 PDMS channel.....	54
4.3 Channel and electrode bonding.....	55
4.4 Removal of PDMS.....	57
V. EXPERIMENTAL RESULT AND FUTURE STUDY.....	58
5.1 Experimental units.....	58
5.2 Preparation of experimental sample.....	59
5.3 Experimental results.....	60
5.4 Future improvement.....	65
5.4.1 Wide channel device.....	66
5.4.2 Feasibility of Blood Cell separation.....	68
5.4.3 New substrate material.....	72

VI. CONCLUSION.....	73
REFERENCES.....	75
APPENDICES.....	81
APPENDIX A: TABLE OF EQUIPMENTS.....	82
APPENDIX B: TABLE OF EXPERIMENTAL MATERIALS.....	83

LIST OF FIGURES

Figure	Page
2-1 Schematic of a Rayleigh wave, copy from Wikipedia. http://en.wikipedia.org/wiki/Rayleigh_wave	7
2-2 Schematic of generating SAW on a piezoelectric substrate.....	8
2-3 Schematic of the SSAW focusing device. The channel width was designed to cover only one pressure node such that beads are focused at that node when the SSAW was generated.	9
2-4 The schematic in (a) indicates the positions of the chosen sites (I–IV) for monitoring the focusing effect. (b–e) are the recorded fluorescent images at sites (I–IV), respectively.	10
2-5 (a) Schematic of the separation mechanism showing particles beginning to translate from the sidewall to the center of the channel due to axial acoustic forces applied to the particles when they enter the working region of the SSAW (site 1). The differing acoustic forces cause differing displacements, repositioning larger particles closer to the channel center and smaller particles farther from the center (site 2). (b) Comparison of forces (normally in PN range) acting on particles at site 1 and site 2, respectively.	12
2-6 Schematic of the separation mechanism and processing. Three different sizes of particles were focused by sheath flow and then separated in SSAW.....	14
2-7 Schematic of the SSAW-based alignment and patterning devices. (a) Distribution of the micro beads of 1D patterning using two parallel IDTs. (b) Distribution of the micro beads of 2D patterning using two orthogonal IDTs.....	15

2-8	Schematic diagram showing the dual-port acoustic wave device. (a) is a top view and (b) a magnified side view along the acoustic beam path, showing acoustic and fluidic displacement and subsequent particle alignment (not to scale).....	17
2-9	(Color online) Micrographs showing sections at 50 × magnification of aligned particles formed by (a) a 32.5 MHz device operating at frequencies of, from top to bottom, 31.0, 31.8, 32.5, 33.6, and 34.4 MHz, and (b) a 96 MHz device operating at frequencies of, from top to bottom, 94.8, 95.6, 96.4, 97.3, and 98.0 MHz. S1–S10 are the distances between four adjacent lines in each case; the average line separation is then given by $S_n / 3$	18
2-10	The four-port acoustic wave device showing acoustic alignment of particles in a fluidic capillary formed from a glass cover-slip, with (1) Marconi 2022E RF signal generator, (2) minicircuits ZHL-1-2W power amplifier, and (3) power splitter.....	19
2-11	Schematic of the hybrid PDMS–SAW chip (top view). (a) If the SAW power is switched off all drops flow along the upper channel. (b) If SAW power is switched on the droplets are driven to the lower channel of the branch. (c) and (d) experimental demonstration when the SAW with a power of 10dBm was switched on and off. The device is 50 mm high and 100 mm in width right before the branch. Flow rates were 100 ml/h for the dispersed phase and 1000 ml/h for the continuous phase.....	20
2-12	Schematic illustrations and corresponding phase contrast micrographs of the surface-acoustic-wave-actuated PDMS hybrid chip for cell sorting. The main channel is hydrodynamically focused by adjusting the flows through two side channels. Without applying a surface acoustic wave the jet of the main channel moves into the left outlet channel due to its lower hydrodynamic resistance. When switching on the SAW, acoustic streaming is induced and deflects the focusing stream into the right channel outlet (ON, right).....	22

2-13 Illustration of acoustic streaming: Due to the different sound velocities in the substrate and in the liquid phases, the SAW energy leaks into the drop at a specific angle, the Rayleigh angle, as it comes into contact with the drop. This gives rise to bulk liquid recirculation (acoustic streaming) within the drop and a body force on the drop itself in the SAW propagation direction. The body force on the drop can causes the drop to deform into an axisymmetrical conical shape and subsequently to translate across the substrate.....24

2-14 Scheme for the assembling of microfluidic devices and the activation of the liquid motion into microchannels: [(a) and (b)] final devices were fabricated by the superposition of a PDMS textured element and a LiNbO₃ substrate layer with IDTs for SAW excitation and detection; (c) DD (direct drive) mode and (d) ID (inverted drive) mode experimental arrangements25

2-15 (a) Photographs of the droplet filling process for DD configuration at different times (t). The SAW was turned on (IDT1) at t=0.00. After 6.96 s, the water droplet at the channel entrance was completely evaporated. (b) Filling process for ID: the SAW was excited (IDT2) at t=0.00 s. After 0.89 s the microchannel was completely filled by water. In the last two frames, the water reservoir was evaporated and the drops present in the microchannel moved in the same direction as SAW propagation.....27

2-16 Photograph of a microfluidic fully controlled low-voltage-driven micro pump in two-dimensional micro channel arrays. The PDMS fluidic layer is aligned to the metallic IDTs. Each IDT is individually labeled by a letter followed by a number: N1–5 and S1–5 are oriented along the X crystallographic orientation of the LiNbO₃ substrate, E1–5 and W1–5 along the Y axis. The scale bar corresponds to 5 mm.....28

3-1 The scheme of forming SSAW field.....30

3-2 Main forces of particles in SSAW field.....31

3-3	Relationship between particle size and time cost. It shows the time of different size polystyrene beads move from anti-pressure node to pressure node in the water in a designed SSAW with fixed applied voltage on the IDTs. The range of particle diameter is from 1 μm to 20 μm . Wavelength is 400 μm and applied voltage is 14 VP-P.	36
3-4	Scheme of design option one.....	38
3-5	Scheme of design option two.....	39
3-6	Scheme of tilted design option two, particles may not be separated.....	39
3-7	Scheme of design option three.....	40
3-8	Forces of particle in SSAW field. Particles can move only when acoustic force is bigger than viscous force. Acoustic force can be increased by increasing the particle size or applying a higher voltage. Wavelength is 400 μm	42
3-9	Acoustic forces applied on different parities in SSAW field.....	43
3-10	Focusing time with different applied voltage. Wavelength is 400 μm	44
3-11	Calculated travel distance of 20 μm and 5 μm polystyrene beads. The dash line shows the difference of two particles' movement at 0.28s, which is about 36 μm Wavelength is 400 μm and applied voltage is 7VP-P.....	45
3-12	Schematic illustrations of IDT.....	46
4-1	Process flow of fabricate electrodes on LiNbO3 Substrate.....	50
4-2	Picture of microfabricated electrode of particle separation device based on SAW. Two pairs of IDTs are fabricated on LiNbO3 substrate	51
4-3	Process flow of making a PDMS channel.....	52

4-4	Photo of channel mode fabricated on a glass substrate.....	54
4-5	Bonding of LiNbO3 substrate and PDMS channel.....	55
4-6	Plasma cleaner PDC- 32G equipped with vacuum pump.....	56
4-7	A picture of the completed particle separation device with bonded connection wires.....	56
5-1	The photo of experimental Units.....	58
5-2	Experimental setup for the particle separation device, particle traces at three positions (a, b, c) were recorded by CCD camera and analyzed.	59
5-3	Mixed particles were inducted into microchannel at position a of Figure 3-2; flow rate was set to be 50 μ L/hour	60
5-4	Particles were focused in a line at the first stage at position b of Figure 3-2; flow rate was set to be 50 μ L/hour, frequency was 9.48 MHz, applied voltage was 20 V_{P-P}	62
5-5	Two types of beads were separated into two lines at the second stage at position c of Figure 3-2. The distance between the two lines reaches the maximum value in the rectangular box which is approximately 36.5 μ m. The distance between the two lines in the circle area is approximately 27.8 μ m. The distance between two analyzed positions in the rectangular box and circle area in the picture is 440 μ m. The applied voltage was 7 V_{P-P} . frequency was 9.48 MHz, The flow rate was set to be 50 μ L/hour, thus the velocity of inlet flow was 860 μ m/s.....	63
5-6	Comparison of predicted result from calculation and the experimental result of rectangular box and circle area are showed in Figure 5-5. The distance of two lines reaches the maximum value at the dash line; the dot-dash line shows the distance of two lines in the circle area.....	64

5-7	Scheme of a wide channel separation device. The channel width was designed as 1200 μm . The design of IDTs is as same as the narrow channel device we presented above.....	66
5-8	Part result of wide channel device. In this picture, beads were first focused into four lines and then separated. This picture is a combination of several pictures shoot by the CCD cameral in a short time. The software makes the initial positions of micro particles (the first picture) as white points and positions of micro particles in next few seconds (the rest pictures) as black points, which shows the tendency of particle movement. The voltage applied at the separation stage is 6.5V. Wavelength is 400 μm . The throughput is 300 $\mu\text{L}/\text{hour}$	67
5-9	Relationship of time and movement of RBC, WBC and Platelet. The dash line shows the distance between three types of blood cells. Dot line shows the time cost of the focusing stage for different blood cells. Wavelength is 300 μm and applied voltage is set to be 30 $V_{\text{P-P}}$	70

LIST OF TABLES

Table	Page
3-1 Parameter of polystyrene beads (particle) and DI water (medium).....	41
3-2 Calculated focusing time.....	44
3-3 Calculated focusing and separating time of different applied voltage.....	47
4-1 Swelling Ratio of PDMS in major organic solvent.....	57
5-1 Throughput of separating with different applied voltage.....	65
5-3 Parameter of blood cells.....	69
5-3 Calculated movement of different blood cells.....	71

CHAPTER I

INTRODUCTION

1.1 Introduction

Recent advances in microfluidics and lab-on-a-chip technologies have enabled many portable biosensors and diagnostic instruments for biomedical research and health care. These devices offer many advantages including reduction in sample and reagent use, high sensitivity, and short processing times. Particle manipulation is an important task for lab-on-a-chip devices. For example, in micro flow cytometers, focusing particles into a narrow stream at the center of the channel is a necessary step for accurately counting and detecting particles [1-3]; additionally separating particles to desired detectors and arranging particles into desired patterns are critically important for a variety of biological and chemical microfluidic sensors such as cell detectors, and DNA and protein sensor array.

Suspended particles in an acoustic wave field are affected by acoustic forces. Acoustic waves generate pressure gradients and acoustic forces in a liquid, which can be used to manipulate suspended particles or liquid medium [4-7]. Acoustic forces are non-contact forces, and are usually harmless to biological objects such as cells. [23] Unlike electrical, optical or magnetic method [8-14], acoustic methods appear to be ideal particle manipulation methods for lab-on-a-

chip devices because they are non-invasive, requires no pretreatment of the particles and work for nearly any type of microscale particles regardless of their optical or charge properties. Recent studies [15-20] demonstrated the separation and manipulation of cells and particles in microfluidic channels, using bulk acoustic waves (BAW) generated by substrate-bonded bulk transducers. However, the generation of bulk acoustic waves requires that the microchannel has excellent acoustic reflection properties [21]. As a result, a bulk acoustic wave is not a good choice for microfluidic devices made of materials with poor acoustic reflection, such as commonly used polydimethylsiloxane (PDMS). Additionally, it is difficult to integrate a bulk transducer into an integrated microsystem. Recently, surface acoustic waves, generated by interdigitated microelectrodes on a piezoelectric substrate, have been demonstrated to focus [21], separate [22], align [23-25], direct micro particles [26, 27] and to manipulate the fluid droplet [29-36] in microchannels. Surface acoustic waves are sound waves that propagate along the surface of an elastic material. Because most energy of surface acoustic wave is confined in the superficial layer, usually within one to two wavelengths normal to the substrate surface, the energy density of SAW is high, making it an effective way for particles and liquid droplets manipulation. Additionally, in comparison to bulk acoustic wave, SAW can be operated as radio frequency, only introduces low-power mechanical vibrations to the liquid medium, and can be easily implemented and miniaturized using soft lithography techniques.

1.2 Motivation

Micro particles to be focused and separated by standing surface acoustic waves (SSAW) have been studied by several teams. [21, 22, 40] They did not do the focusing or separation all by surface acoustic waves simultaneously. Sheath flow was induced to achieve the focusing of micro particles in their researches.

The sheath flow is an easy and convenient method to focus particles, and it can adjust the width of the focusing line by adjusting the different velocities of sheath flow and target, micro particles solution. However, the sheath flow may cause some problems for it induces additional fluid besides of target and needs more inlets. That is feasible for the polystyrene micro particles. But if your targets are cells or blood etc, the sheath flow will increase the risk of contaminating your targets. Therefore, the velocity of the sheath flow has to be much greater than the velocity of your target; it may damage the bonding between the channel and the SAW substrate. And it will focus your targets in a tiny line with a small width, so the throughput of your target is doubtful. The maximum throughput they gotten is less than 20 $\mu\text{l}/\text{hour}$. [40] Moreover, these devices need more pumps to induce sheath flow and targets separately, which can make the device much more complex and infect its reliability as well.

1.3 Objective

This study is to design and manufacture a two stage microfluidic separation device to separate microscale particles by size only based on

standing surface acoustic waves. At the first stage, all particles are designed to focus in one line, which is the pressure node of the SSAW field. At the second stage, the larger particles will move quickly and travel a larger lateral displacement than smaller ones within a fixed time; the particles are hence separated. This device should only utilize the surface acoustic wave in both stages; it will not induce any sheath flow. And the width of the channel should not have distinct change in the working area; otherwise it may confuse us about the effect of dimension change in the separation compared to the effect of SSAW field. It is expected to get a higher throughput compared to the existing SSAW separation devices whose throughputs are less than 20 $\mu\text{l}/\text{hour}$.

1.4 Significance of the study

This work presents a good method to achieve the alignment, focusing and separation of microscale particles on a lab-on-a-chip (LOC) device. It just utilizes SSAW field to accomplish its function, without any kinds of sheath flow or other factors. SAW based techniques are non-invasive, require no pretreatment of the particles and work for nearly any type of microscale particles regardless of their optical or surface properties, and are usually harmless to biological objects such as cells. More important, SAW based particle manipulation permits the use of a relatively large microfluidic channel, allowing high throughput and less clogging. With the additional advantages of fast control speed, high energy density, low power intensity, and compatibility with soft-lithography micromachining, SAW based particle manipulation techniques appear to be ideal for lab-on-a-chip

devices for a variety of biological applications and medical researches such as cell detection, drug screening and tissue engineering.

1.5 Specific goals

a. Design and fabricate a two-stage particle separation device based on surface acoustic waves to continuously separate micro particles such as 5 μm polystyrene beads and 20 μm polystyrene beads.

b. Focus all micro particles with different size on one line at the first stage with surface acoustic waves in a short time, no particles should be out of designed lines.

c. Separate micro particles of different size into different lines at the second stage with surface acoustic wave quickly.

d. Attempt to use a wide channel or multi-channel to enhance the throughput and efficiency. Study the effect of the channel width, and compare it to the single channel device.

e. Use microscope to observe the movement of micro particles and take pictures or make short movies. Find the best applied voltage and frequency of signal to get the best separation result and the highest throughput.

1.6 Outline

In this thesis, a particle separation device based on surface acoustic wave is presented. The outline is as follows:

- Chapter 2 gives an introduction of SAW and the prior work of SAW device used in particles and droplets manipulation.
- Chapter 3 explains the theory of the design; compares several designs and predicts the experimental result by numerical model.
- Chapter 4 describes the fabrication process of this micro particles separation device and introduces a new method of completely removing the bonding between PDMS channel and substrate, which was considered as irreversible.
- Chapter 5 shows the experimental setup and results obtained from the testing of the device, then analyze is followed. Future improvements and application of this separator are discussed as well.
- Chapter 6 is the conclusion part of this thesis.

CHAPTER II
BACKGROUND AND LITERATURE REVIEW

2.1 Introduction of SAW

The first kind of surface acoustic waves, Rayleigh wave was first explained by Lord Rayleigh, after whom they were named, when he was studying the earthquake in 1885. Rayleigh wave travels near the surface of solids. As 90% energy of Rayleigh wave was confined within a wavelength depth from the surface, the energy density of SAW is high, making it an effective way for particles and liquid droplets manipulation.

Rayleigh Wave

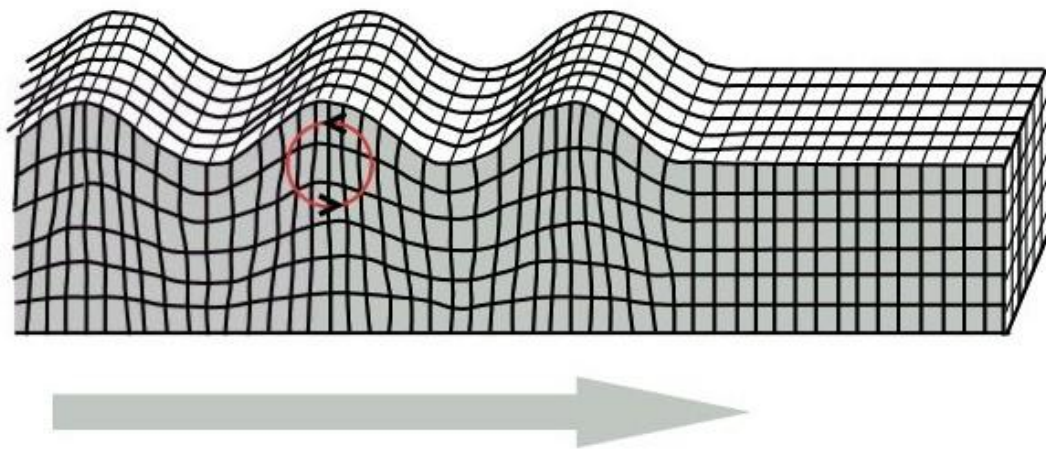


Figure 2-1 Schematic of a Rayleigh wave, copy from Wikipedia.

http://en.wikipedia.org/wiki/Rayleigh_wave

Besides Rayleigh wave, surface acoustic waves also include Shear-horizontal surface acoustic waves [SH-SAW], surface-skimming bulk waves [SSBW], leaky SAW, Love Waves, Scholte waves, pseudo-SAW and many others, which are used in applications in lieu of the Rayleigh wave. [4, 41]

Interdigital Transducer (IDT) was firstly reported in 1965 by White and Voltmer for generating SAWs on a piezoelectric substrate. IDT was formed by two identical combs-like metal electrodes whose fingers are located in a periodic alternating pattern. When a RF signal was applied on the IDT, because of the inverse piezoelectric effect of the substrate, the surface will generate an alternate vibration of shrink and tension, and then one kind of SAW, Rayleigh wave occurs.

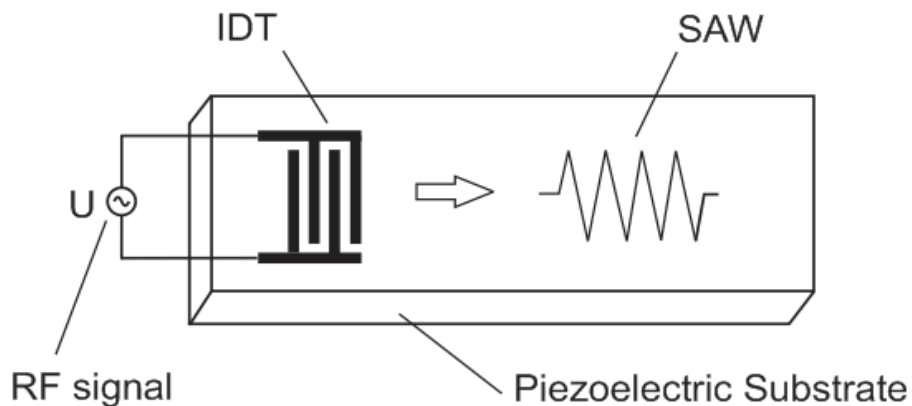


Figure 2-2 Schematic of generating SAW on a piezoelectric substrate

2.2. Application of SAW

Nowadays, surface acoustic wave generated by IDT have been widely used in particles and droplets manipulation including particle focusing and

separation, particle alignment and patterning, particle directing, and liquid droplet delivery. [42]

2.2.1 Particle focusing and separating

Standing surface acoustic waves (SSAW) can be formed by the interference of two series of identical surface acoustic waves propagated in opposite directions. SSAW generate periodic pressure nodes (minimum pressure) and anti-pressure nodes (maximum pressure) in a fluid. The positions of the pressure and anti-pressure nodes can be controlled and used for particle manipulation by adjusting the acoustic wavelength.

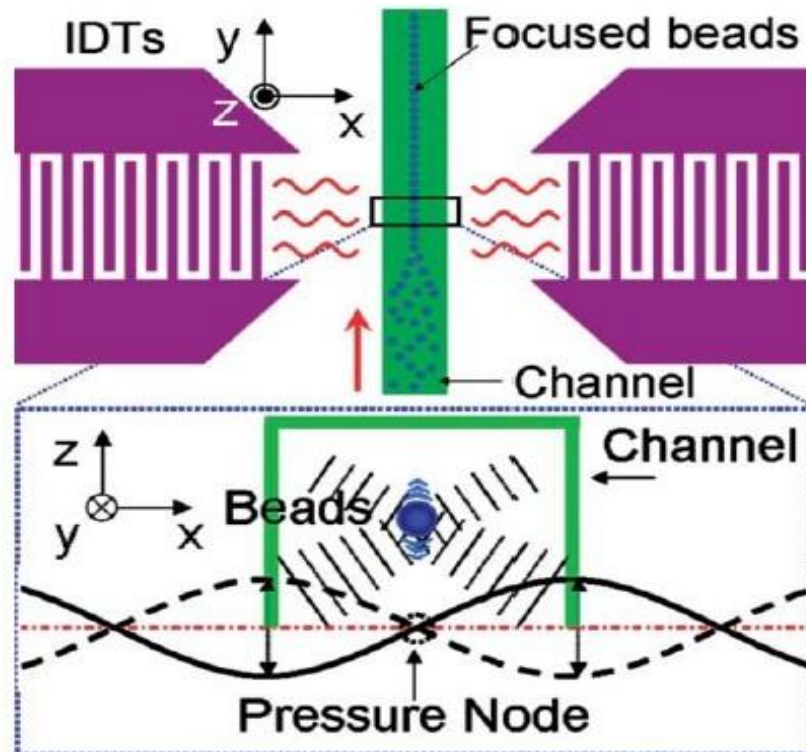


Figure 2-3 Schematic of the SSAW focusing device. The channel width was designed to cover only one pressure node such that beads are focused at that

node when the SSAW was generated. Reprinted from Shi et al. [21] with permission from Royal Society of Chemistry.

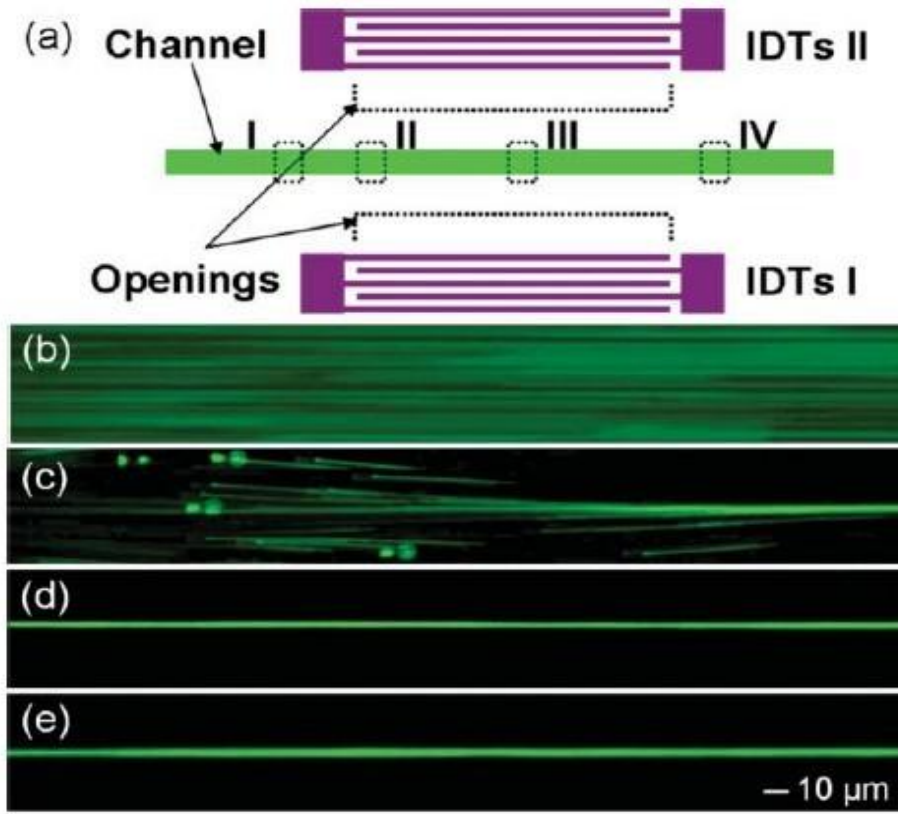


Figure 2-4 The schematic in (a) indicates the positions of the chosen sites (I–IV) for monitoring the focusing effect. (b–e) are the recorded fluorescent images at sites (I–IV), respectively. Reprinted from Shi et al. [21] with permission from Royal Society of Chemistry.

Shi et al. [21] developed a microfluidic particle focusing device using standing surface acoustic waves. Figure 1 shows the schematic of the device. Two identical interdigital transducers (IDTs) were fabricated on a piezoelectric

(LiNbO₃) substrate, and a microfluidic channel was aligned between the IDTs. The microchannel served as an acoustic resonator. When the two IDTs were stimulated with RF signals of equal magnitude but 180° out of phase, two series of surface acoustic waves propagated in opposite directions along the surface of the piezoelectric substrate toward the particle solution inside the microchannel. When the surface acoustic wave reached the fluid in the microchannel, leakage waves in longitudinal mode were generated inside the fluid, resulting in the pressure fluctuation. The interference of the two acoustic waves formed a standing acoustic wave that generated a periodic distribution of pressure nodes and anti-nodes in the microchannel. Because solid particles have positive acoustic contrast factors, the acoustic radiation forces caused by the pressure fluctuations moved the particles toward the pressure nodes in the SSAW field.

By choosing the width of the microchannel to be the half-wavelength of the SSAW, the channel contained one pressure node located in the centerline of the channel (Figure 2-3). Thus, particles aggregated at the centerline of the microchannel. Using a microchannel with a width and depth of 50 μm and a length of 1.3 cm, Shi et al. observed that 1.9 μm-diameter polystyrene beads were focused into a narrow stream in the center of the microchannel within 4.5 ms(Figure 2-4).

Standing surface acoustic waves can also be employed for particle separation. The acoustic force that pushes the particles to move from anti-pressure node to pressure node in a SSAW field is dependent on the particle size and compressibility. Within a fixed time, larger particles travel a larger

lateral displacement than smaller ones. Therefore by tuning the flow velocity, channel length, and SAW power particles with different size travel different distances in the channel width direction; the particles are hence separated. Shi et al. [22] reported a simple device using SSAW to continuously separate particles in a micro fluidic channel. At the inlet, a sheath flow was used to push the particle mixture streams near the channel wall. By applying RF signals to the IDTs, the acoustic forces drove particles to move to the pressure node, the centerline of the microchannel. Particles were repositioned with different lateral displacements, separated to multiple streams and guided to collection outlets. Their testing showed that $0.87\ \mu\text{m}$ and $4.17\ \mu\text{m}$ latex particles can be separated in 360 ms.

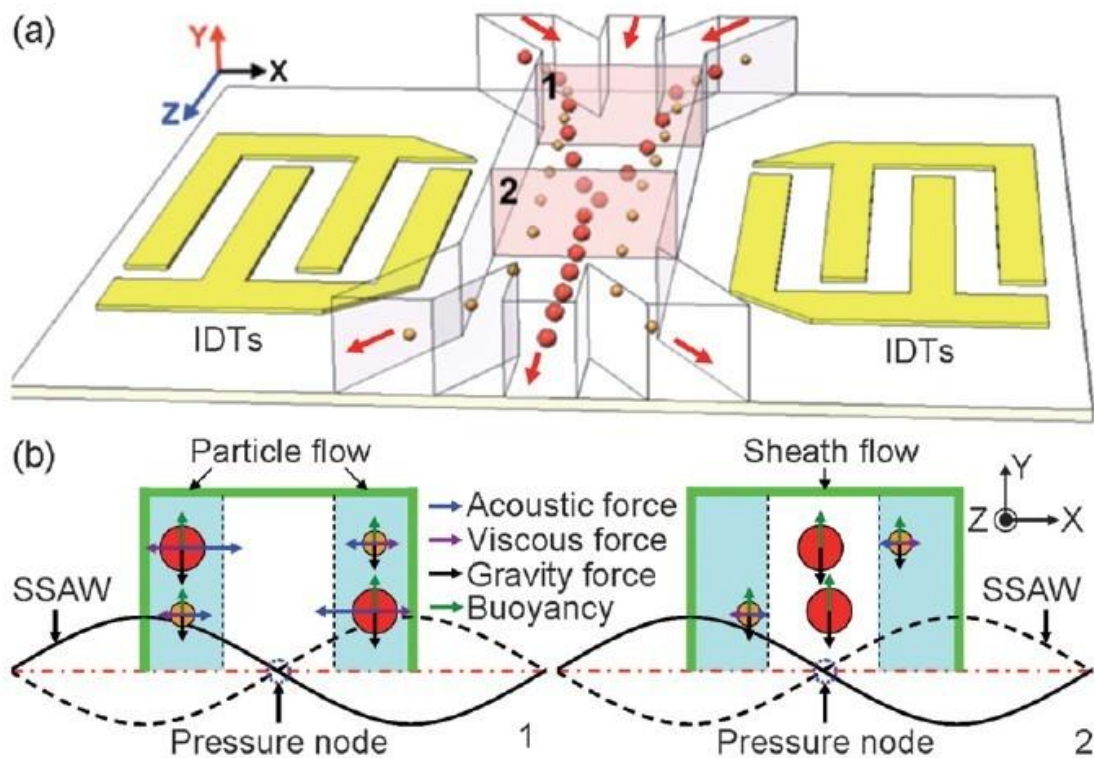


Figure 2-5 (a) Schematic of the separation mechanism showing particles beginning to translate from the sidewall to the center of the channel due to axial acoustic forces applied to the particles when they enter the working region of the SSAW (site 1). The differing acoustic forces cause differing displacements, repositioning larger particles closer to the channel center and smaller particles farther from the center (site 2). (b) Comparison of forces (normally in PN range) acting on particles at site 1 and site 2, respectively. Reprinted from Shi et al. [22] with permission from Royal Society of Chemistry.

Recently, Nam et al. [40] developed a similar device using SSAW to continuously separate particles in a micro fluidic channel. Three different sizes of particles (1, 5, 10 μm) were first pushed to the centerline of microchannel by using sheath flow, and then were separated in the course of moving to the side walls of microchannel under lateral acoustic radiation forces (because of SSAWs). The highest throughput they got was 0.3 $\mu\text{L}/\text{min}$, while the stable result was gotten with a throughput of 0.22 $\mu\text{L}/\text{min}$.

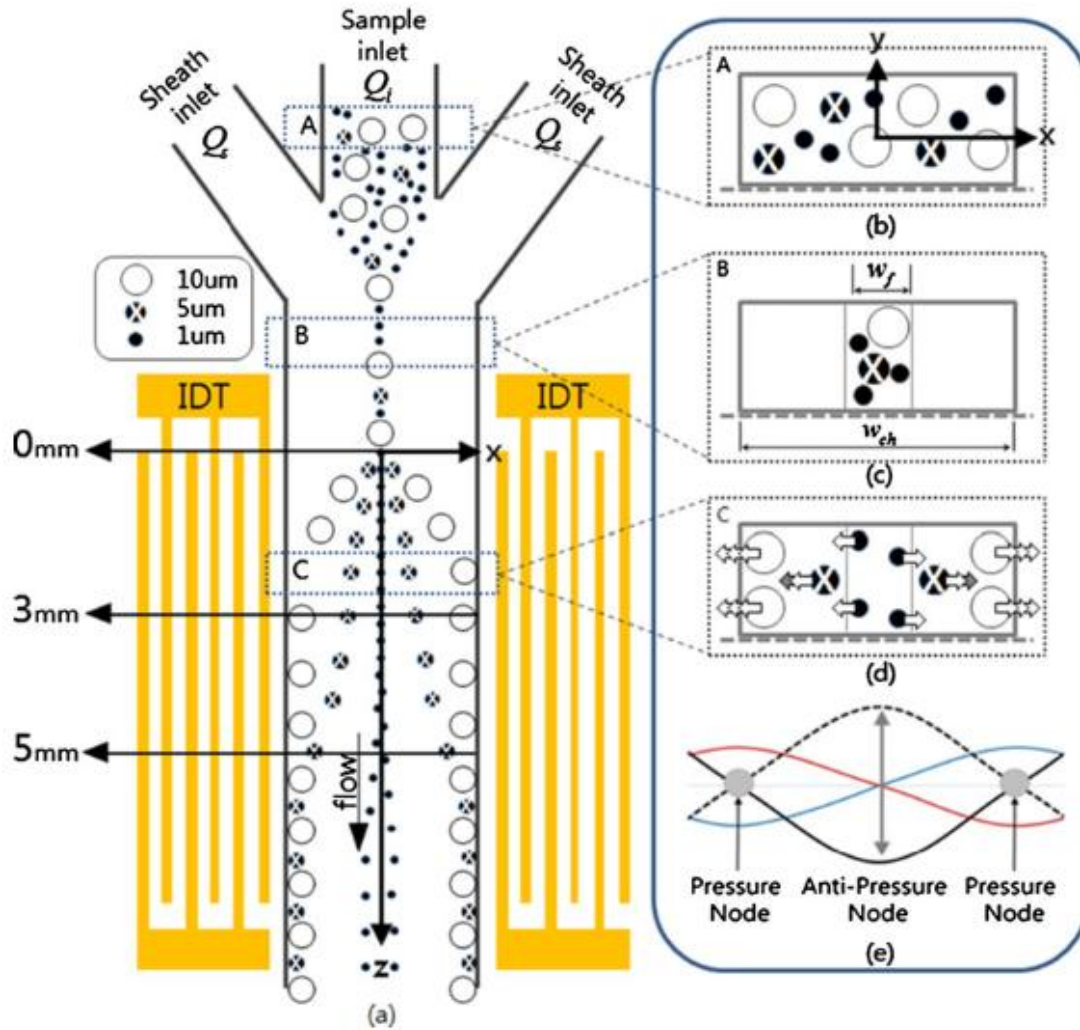


Figure 2-6 Schematic of the separation mechanism and processing. Three different sizes of particles were focused by sheath flow and then separated in SSAW. Copy from Nam et al. [40]

2.2.2 Particle alignment and patterning

Shi et al. [23] had demonstrated “acoustic tweezers” for particle alignment and patterning using standing surface acoustic waves. Figure 2-7 illustrates the working mechanism of the acoustic tweezers.

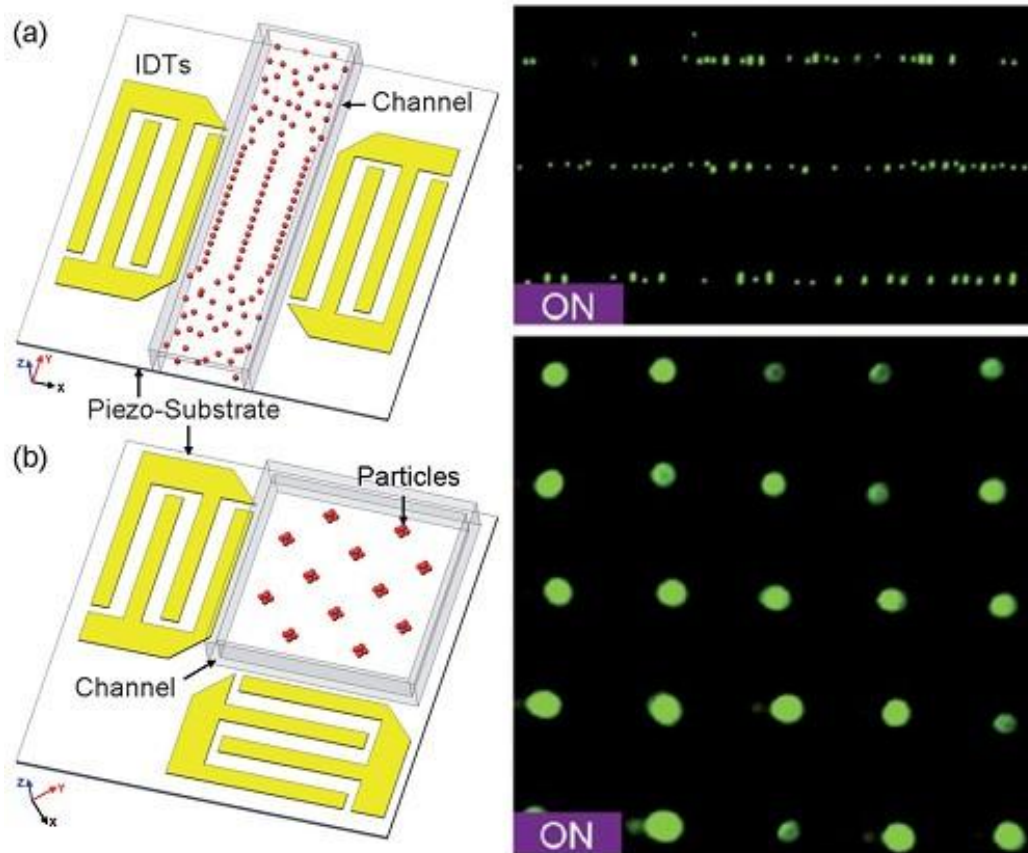


Figure 2-7 Schematic of the SSAW-based alignment and patterning devices. (a) Distribution of the micro beads of 1D patterning using two parallel IDTs. (b) Distribution of the micro beads of 2D patterning using two orthogonal IDTs. Reprinted from Shi et al. [23] with permission from Royal Society of Chemistry.

Two series of identical SAWs propagating either in the opposite or orthogonal directions formed a standing surface acoustic wave, and a periodic distribution of pressure nodes and anti-pressure nodes inside a microchannel. In a one-dimensional SSAW field, the pressure nodes were located at multiple lines parallel to the central line of the microchannel; therefore suspended particles were aligned along these lines. In a two dimension SSAW field, a 2-D array of

pressure nodes were formed; suspended particles moved and aggregated at the pressure nodes, forming 2-D patterns of particles. Alignment and patterning of 1.9 μm microscale latex particles, bRBC and E. coli cells using the acoustic tweezers were successfully demonstrated after applying a RF excitation to the pair of IDTs as well with a proof that the applied standing surface acoustic waves is harmless to cells. By tuning the wavelength, the spacing of the 1-D and 2-D particle patterns can be adjusted.

Wood et al. reported similar devices that utilized SSAW to align micro latex particles along a series of lines [24], and organize particles into 2-D array [25]. Figure 2-8 is the schematic diagram of the 1-D SSAW device for particle alignment.

Two opposing IDTs, fabricated on 128° Y-rotated LiNbO_3 substrate, were located on either side of a microfluidic channel with suspended latex particles. When identical RF signals were applied to the pair of IDTs, the resulted SSAW formed a periodic distribution of pressure nodes consisting of a series of lines within the fluidic channel. The pressure gradient forced the particles to aggregate at the pressure-nodes, aligning particles at the pressure node lines. The distance between adjacent alignment lines was equal to half of the SAW wavelength. The testing demonstrated that the distance between the lines of aligned particles can be adjusted by changing the RF excitation frequency.

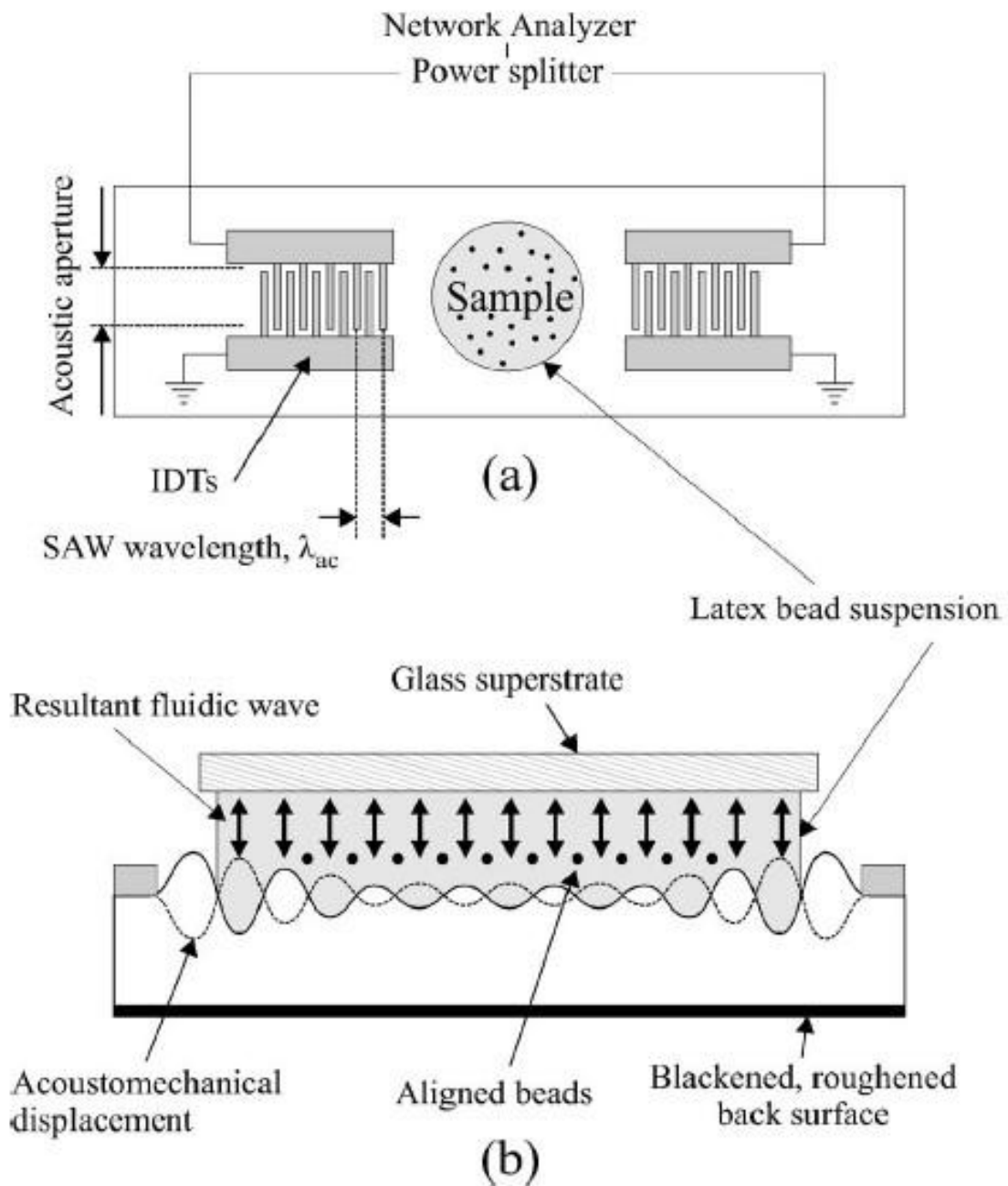


Figure 2-8 Schematic diagram showing the dual-port acoustic wave device. (a) is a top view and (b) a magnified side view along the acoustic beam path, showing acoustic and fluidic displacement and subsequent particle alignment (not to

scale). Reprinted from C. D. Wood et al. [24] with permission from American Institute of Physics.

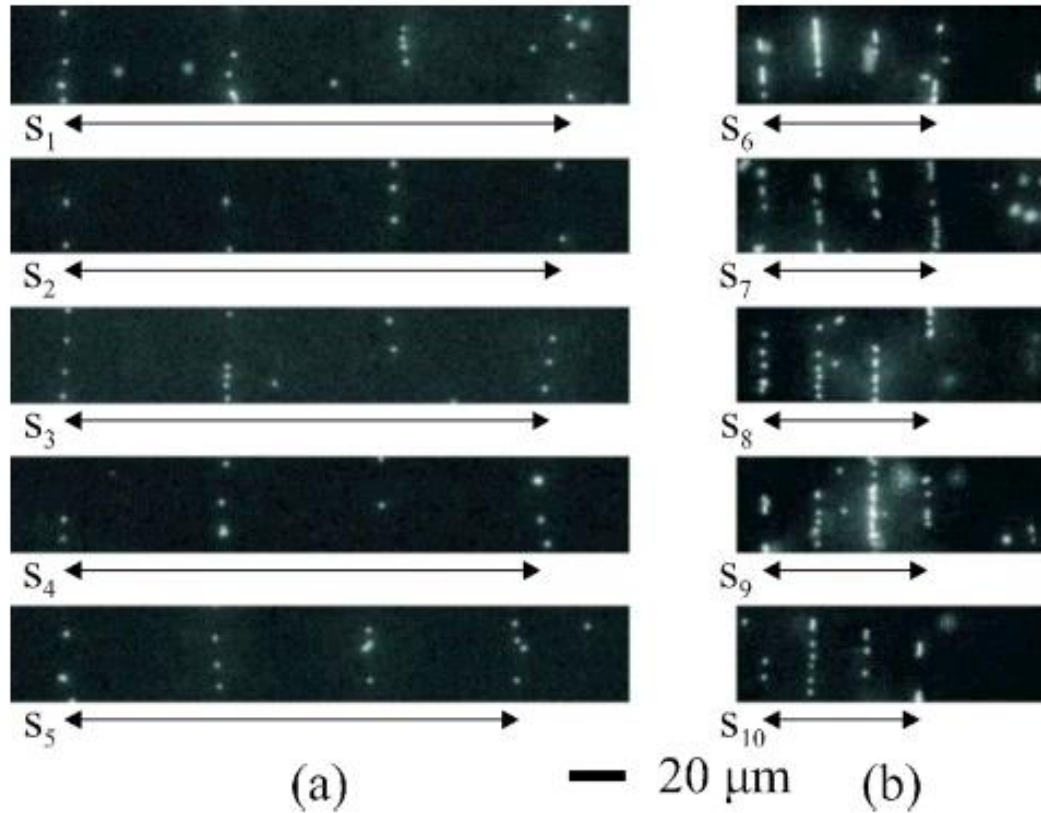


Figure 2-9 (Color online) Micrographs showing sections at $50\times$ magnification of aligned particles formed by (a) a 32.5 MHz device operating at frequencies of, from top to bottom, 31.0, 31.8, 32.5, 33.6, and 34.4 MHz, and (b) a 96 MHz device operating at frequencies of, from top to bottom, 94.8, 95.6, 96.4, 97.3, and 98.0 MHz. S_1 – S_{10} are the distances between four adjacent lines in each case; the average line separation is then given by $S_n / 3$. Reprinted from C. D. Wood et al. [24] with permission from American Institute of Physics.

Later on, Wood et al. [25] used two orthogonal pairs of counter propagating traveling SAWs, generated on LiNbO₃ piezoelectric substrate, to produce a two-dimensional patterning of pressure nodes, which drives the particles to form a 2-D pattern. Using a frequency of 32.5 MHz, a pattern consisting of 456 particle aggregation nodes was formed. The distance between escrow and column was equal to half of the SAW wavelength. By tuning the SAW frequency, the distance can be adjusted.

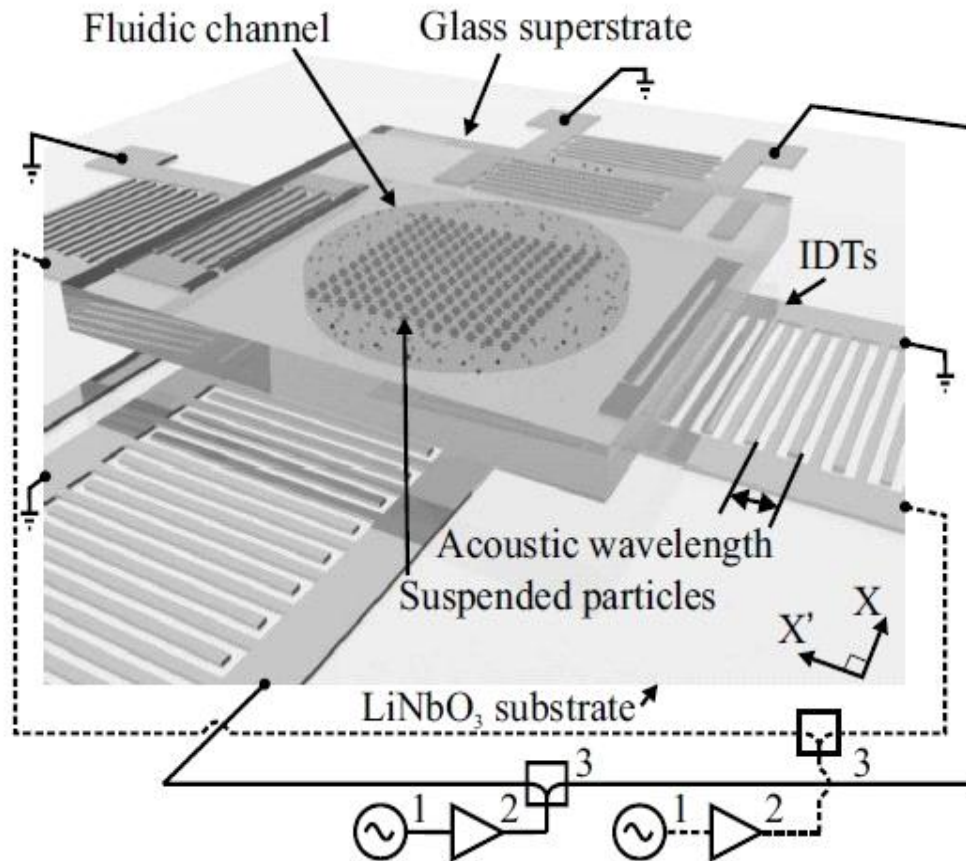


Figure 2-10 The four-port acoustic wave device showing acoustic alignment of particles in a fluidic capillary formed from a glass cover-slip, with (1) Marconi 2022E RF signal generator, (2) minicircuits ZHL-1-2W power amplifier, and (3)

power splitter. Reprinted from C. D. Wood et al. [25] with permission from American Institute of Physics.

2.2.3 Particle directing

Acoustic streaming, resulted from surface acoustic wave excitations at a high frequency, can be used to actuate bulk fluid. Acoustic streaming has recently been applied to enhance mixing, pumping and agitation in open fluidic droplets and was reviewed extensively by Yeo et al [7]. Unlike using standing surface acoustic waves, SAW actuated acoustic streaming does not rely on compressibility difference between particles and the medium fluid.

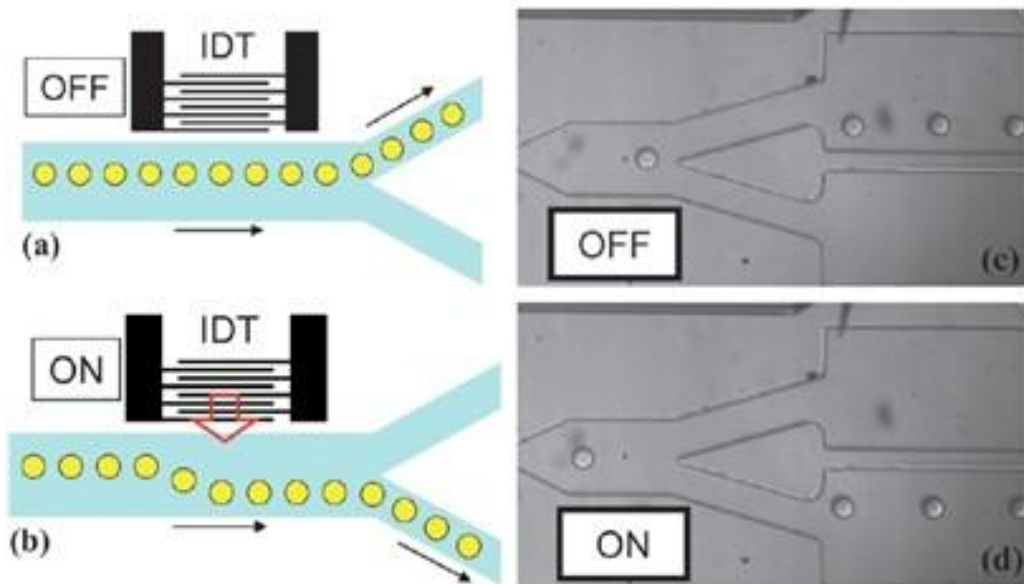


Figure 2-11 Schematic of the hybrid PDMS–SAW chip (top view). (a) If the SAW power is switched off all drops flow along the upper channel. (b) If SAW power is switched on the droplets are driven to the lower channel of the branch. (c) and (d) experimental demonstration when the SAW with a power of 10dBm was switched

on and off. The device is 50 mm high and 100 mm in width right before the branch. Flow rates were 100 ml/h for the dispersed phase and 1000 ml/h for the continuous phase. Reprinted from Franke et al. [27] with permission from The Royal Society of Chemistry.

Franke et al. [26] demonstrated that the application of SAW can direct movements of water droplets in oil and polyacrylamide particles in water respectively, in a microfluidic channel (Figure 4(a) and (b)). Surface acoustic waves were generated by a single IDT fabricated on a 128° Y-cut LiNbO₃ substrate. The IDT was located on one side of a 100 μm wide microchannel. Without applying a RF excitation to the IDT (Figure 4(a)), 20 μm water droplets generated slightly above the centerline of the channel in fluorocarbon oil flowed along the upper channel because of the lower flow impedance. By applying a 140MHz RF excitation, the acoustic streaming drove the droplets to the lower channel (Figure 4(b)). Later on, Franke et al [26] demonstrated the polyacrylamide particles were directed to the lower channel by SAW at a radio frequency (140MHz). This device allows a non-labeling and fast approach for directing particles and can be used for particle detection and sorting systems.

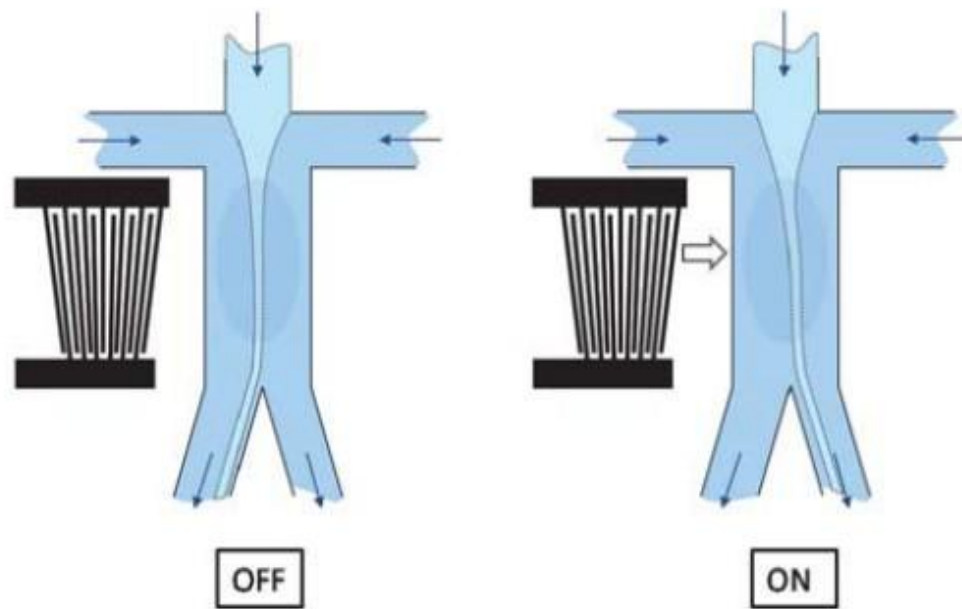


Figure 2-12 Schematic illustrations and corresponding phase contrast micrographs of the surface-acoustic-wave-actuated PDMS hybrid chip for cell sorting. The main channel is hydrodynamically focused by adjusting the flows through two side channels. Without applying a surface acoustic wave the jet of the main channel moves into the left outlet channel due to its lower hydrodynamic resistance. When switching on the SAW, acoustic streaming is induced and deflects the focusing stream into the right channel outlet (ON, right). Reprinted from Franke et al. [27] with permission from The Royal Society of Chemistry.

Recently T. Franke et al. [27] demonstrated an improved microfluidic device for cell sorting in continuous flow, using SAW generated by a tapered IDT (Figure 4(c)). The tapered shape of the IDT with decreasing finger spacing

defined a narrow path width for SAW propagation because only one finger spacing satisfied the acoustic resonance condition at one position.

The main channel of this device was hydrodynamically focused slightly toward the left side at inlet by adjusting the flow rates through two side channels. Without applying an AC excitation to the IDT, the focused stream was guided to the left outlet channel. When switching on the AC excitation, acoustic streaming induced by SAW deflected the focused stream to the propagating direction, thus directed cells to the right outlet channel. HaCaT cells, murine fibroblasts L929 cells and MV3 melanoma cells were sorted well with this device, without a need to enclose cells in droplets or labeling them prior to sorting. The cells can be periodically sorted into collection channels by switching the SAW on and off; a 2 kHz sorting rate with 100% sorting efficiency was demonstrated. A viability test indicated 94% viability for sorted cells as compared to a control reference of 97% viability.

2.2.4 Liquid droplet delivery

Surface acoustic waves can be used to manipulate a liquid droplet placed within the propagation path of SAWs on a piezoelectric substrate owing to the fluid-SAW coupling. Because of the mismatch between the sound velocities in the piezoelectric substrate and in the liquid, the SAW energy leaks into the drop, known as a leaky surface acoustic wave (Leaky-SAW). Depending on the power of the SAW, the Leaky-SAW can cause a longitudinal pressure wave front, induce bulk liquid recirculation within the droplet, or cause a body force on the

droplet along the SAW propagation that causes the droplet to deform into an axisymmetrical conical shape and subsequently to translate across the substrate [7].

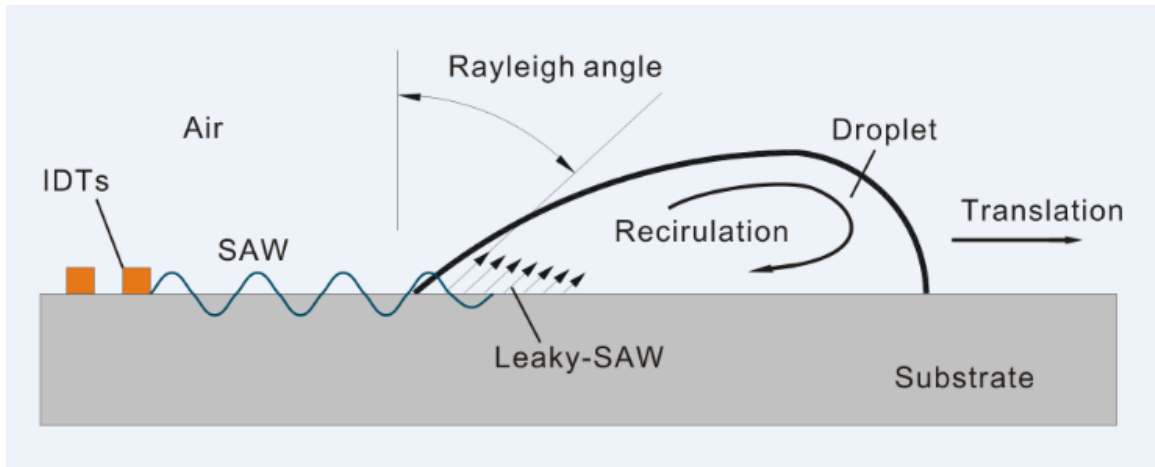


Figure 2-13 Illustration of acoustic streaming: Due to the different sound velocities in the substrate and in the liquid phases, the SAW energy leaks into the drop at a specific angle, the Rayleigh angle, as it comes into contact with the drop. This gives rise to bulk liquid recirculation (acoustic streaming) within the drop and a body force on the drop itself in the SAW propagation direction. The body force on the drop can cause the drop to deform into an axisymmetrical conical shape and subsequently to translate across the substrate.

This effect, known as acoustic streaming, has been utilized for a variety of droplet manipulations, including droplet vibration, droplet translation, micro pumping and mixing, microcentrifugation, jetting, and atomization. The working principles of these manipulation schemes and their derivatives have been discussed thoroughly in Ref. [7]. If the SAW power is sufficient, a liquid droplet in the propagating path can be translated to the desired location with a moving

speed as high as 10 cm/s, which is one to two magnitude higher than the speeds achieved by other microfluidic actuation mechanisms, such as electrowetting. Due to the simple structure and fast speed, SAW based drop delivery has received extensive attentions. A couple of microfluidic droplet delivery devices [28-32] have been demonstrated very recently using bulk LiNbO_3 substrate. Bulk LiNbO_3 substrate has been widely used in SAW devices, but it is expensive, fragile and cannot be fabricated using micromachining. Du et al. [33] used octadecyltrichlorosilane (OTS) treated thin film ZnO deposited on Si substrates as piezoelectric materials for droplet delivery. Compared to LiNbO_3 , thin film ZnO is cheaper, can be micromachined and permits a higher applied voltage (> 70V). The device can manipulate liquid droplet with a volume up to $50\mu\text{l}$.

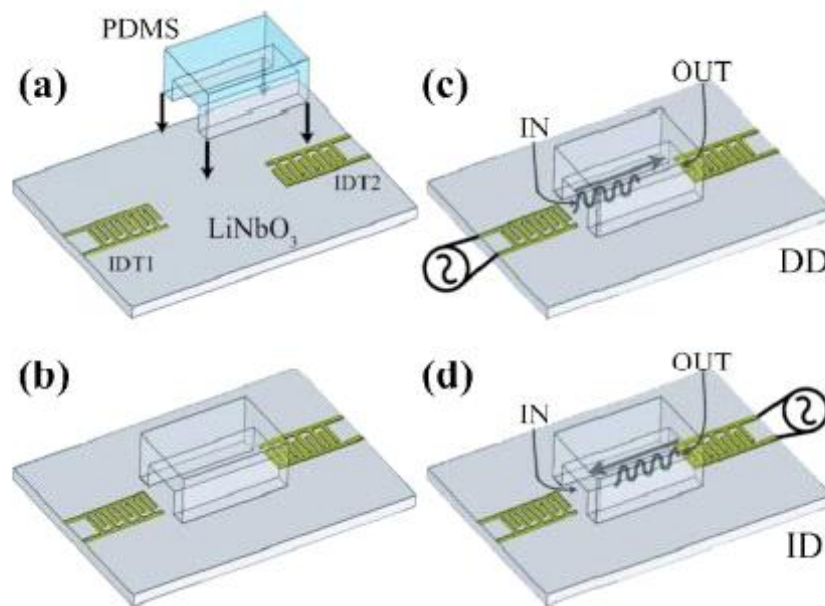


Figure 2-14 Scheme for the assembling of microfluidic devices and the activation of the liquid motion into microchannels: [(a) and (b)] final devices were fabricated by the superposition of a PDMS textured element and a LiNbO_3 substrate layer

with IDTs for SAW excitation and detection; (c) DD (direct drive) mode and (d) ID (inverted drive) mode experimental arrangements. Reprinted from Cecchini et al. [34] with permission from American Institute of Physics.

In addition to delivering liquid droplet in an open area, SAW can also be used to translate liquid droplet or segments in confined microchannels. Cecchini's group [34] developed PDMS-LiNBO₃ SAW devices for droplet control in microchannels as illustrated in Figure 2-14. Two IDTs were fabricated at the inlet and the outlet of the microchannel. A liquid droplet was placed between one IDT and the channel inlet.

Two operation modes were tested: 1) SAW were excited from the IDT near the channel inlet and hence propagated from the inlet to the outlet (direct drive mode, see Figure 2-14(c)), and 2) SAW were excited from the IDT near the channel outlet and propagated from outlet toward inlet (inverted drive mode, see Figure 2-14(d)). For direct drive mode, after switching on SAW with an excitation power of approximately 20dBm, the droplet was driven into the PDMS microchannel with a relatively slow filling speed of the order of tens of $\mu\text{m/s}$. This is because with such a high SAW power, significant droplet atomization occurred at the droplet outside of the channel where the SAW power was maximum, leading to fast evaporation of the droplet and preventing the filling of the microchannel. In contrast, for inverted drive mode, a fast liquid droplet translation into the microchannel was observed with even less SAW power ($\sim 14\text{dBm}$). This is because significant droplet atomization occurred at the

meniscus liquid-air interface where the SAW power was maximum, forming many small liquid particles in front of the interface; the continuous coalescence of the small liquid particles with the meniscus liquid interface because of the acoustic streaming effect determined the advancement of the liquid interface, resulting in a net fluid movement in the direction opposite to the SAW propagation [34, 35]. Experiments showed that the liquid transport velocity reached 1.24 mm/s using inverted drive mode, which was nearly two orders higher than the droplet velocity using direct drive mode.

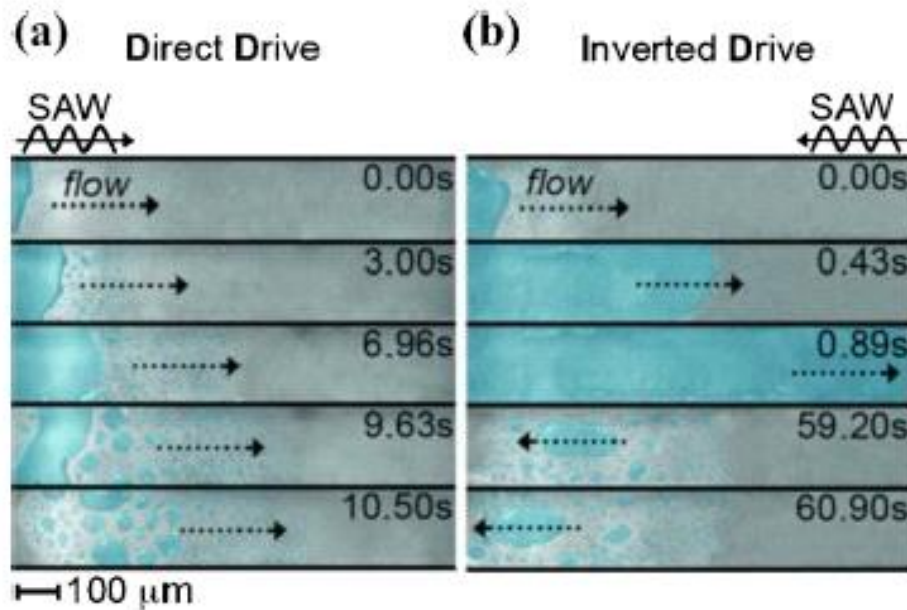


Figure 2-15 (a) Photographs of the droplet filling process for DD configuration at different times (t). The SAW was turned on (IDT1) at $t=0.00$. After 6.96 s, the water droplet at the channel entrance was completely evaporated. (b) Filling process for ID: the SAW was excited (IDT2) at $t=0.00$ s. After 0.89 s the microchannel was completely filled by water. In the last two frames, the water reservoir was evaporated and the drops present in the microchannel moved in

the same direction as SAW propagation. Reprinted from Cecchini et al. [34] with permission from American Institute of Physics.

Based on the above droplet translation mechanism using inverted SAW-drive mode, Masini et al. [36] introduced a fully controlled low-voltage-driven micro pump in two-dimensional micro channel arrays. The device consists of a 5×5 orthogonal array of PDMS microchannels fabricated on a LiNbO₃ substrate, and 20 IDTs for SAW excitation. By selectively generating single or multiple SAWs, fluid droplets can be delivered to selected positions of the microchannel grid. Fluid extraction, deviation, splitting, and simultaneous multichannel filling were demonstrated. The translation speed of a fluid droplet can reach up to 200 μm/s.

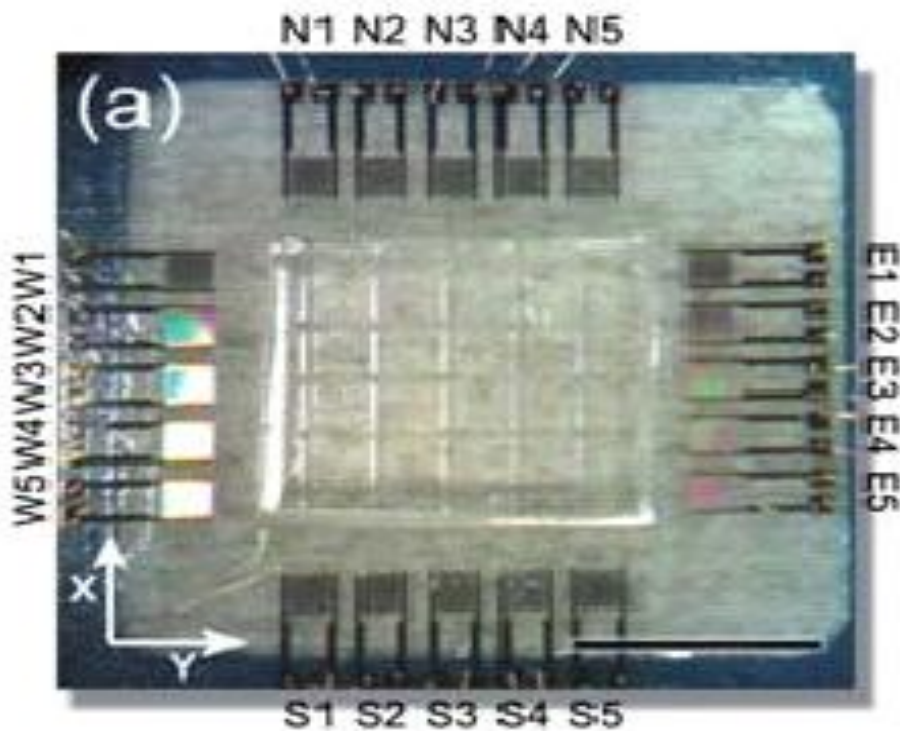


Figure 2-16 Photograph of a microfluidic fully controlled low-voltage-driven micro pump in two-dimensional micro channel arrays. The PDMS fluidic layer is aligned to the metallic IDTs. Each IDT is individually labeled by a letter followed by a number: N1–5 and S1–5 are oriented along the X crystallographic orientation of the LiNbO_3 substrate, E1–5 and W1–5 along the Y axis. The scale bar corresponds to 5 mm. Reprinted from Masini et al. [36] with permission from The Royal Society of Chemistry.

CHAPTER III

DESIGN AND CALCULATION

3.1 Theory Analysis

As discussed in Chapter 2, IDT, formed by two identical combs-like metal electrodes whose fingers are located in a periodic alternating pattern, can generate SAWs on a piezoelectric substrate while applying a RF signal. Acoustic is one kind of vibrations and can generate force on both of the particles and medium in the acoustic field. This force depends on the property of the medium and the particles.

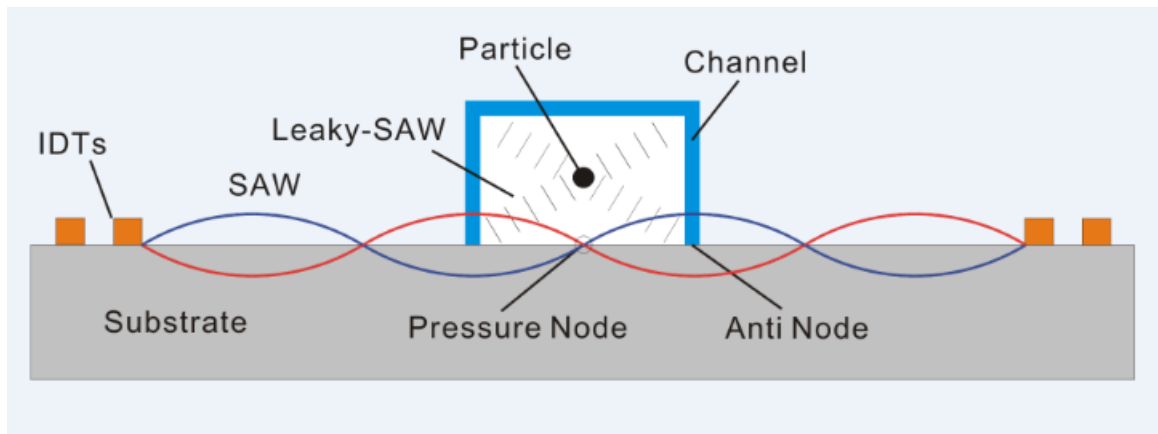


Figure 3-1 The scheme of forming SSAW field

When there are two series of identical-frequency surface acoustic waves that propagated in the opposite directions, it will form a standing surface acoustic

wave. In the SSAW field, some particles will move to the pressure node and others will move to the anti-pressure node. The movement depends on the property of medium and particles. Normally, the force applied on the particles by SSAW field is much bigger than that applied on the medium. So at most time, particles will move to the pressure node. Sometimes the force applied on the particles may be smaller than the one applied on the medium. Then the particles will move to the anti-pressure node.

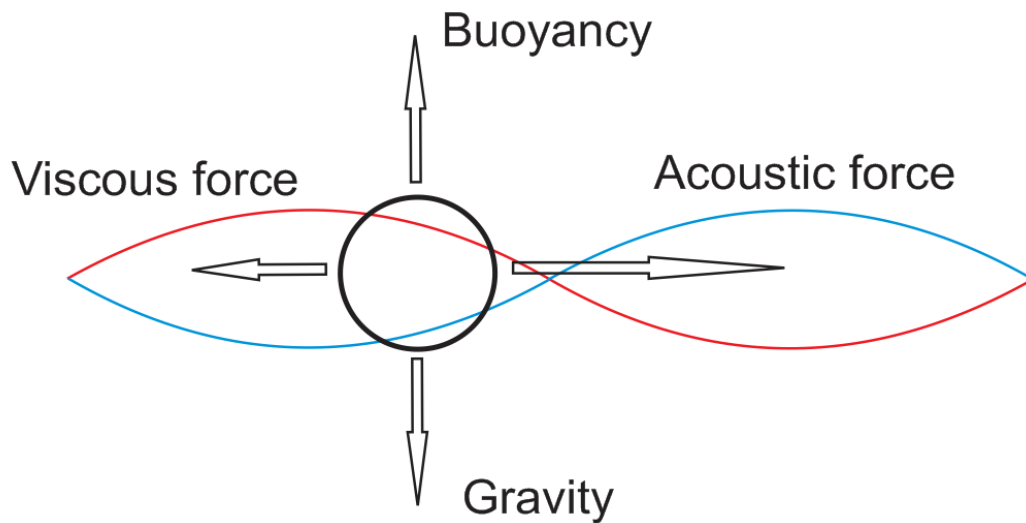


Figure 3-2 Main forces of particles in SSAW field

Particles in the SSAW field majorly come under six types of forces, including acoustic force generated by SSAW field, viscous force generated by medium, gravity, buoyancy, force among particles and force between particle and channel. Force among particles can be reduced by surfactant; and force between particle and channel would be so small that can be ignored when particles were far away from the channel wall, for instance, in the central area of channel.

Gravity and buoyancy balance each other; they do not affect particle movement in a SSAW field. Therefore in the period of particle congregation and separation, acoustic force and the viscous force are the dominating forces and should be considered in design and calculation.

For micro components, including micro particles and cells, their dimensions are much smaller than the wavelength of microwave; the acoustic diffraction will occur; as a result, irregular shape particle can be simplified as a compressible sphere. [43]

The standing wave can be presented as:

$$y = A \sin\left(\frac{2\pi z}{\lambda} + \frac{\varphi}{2}\right) \cos\left(\frac{2\pi t}{T} + \frac{\varphi}{2}\right)$$

And it can be rewritten in term of pressure:

$$P = p \sin(2kz) \cos(2\omega t)$$

Where,

$$\delta P = \rho \phi_1 - \frac{1}{2} \rho u_1^2 + \frac{1}{2} \frac{\rho}{c^2} \phi_1^2$$

$$\Delta \phi_1 = \frac{1}{c^2} \frac{\partial^2 \phi_1}{\partial t^2}$$

Where k is the wave vector, ρ the density of the medium, c the sound velocity, \mathbf{u}_1 the first order velocity ($= -\nabla \phi_1$), and ϕ_1 the first order velocity potential.

The radiation pressure on a moving boundary can be calculated:

$$\langle P \rangle = \langle P_{\mu\nu} \rangle + \langle P_{\mu\theta} \rangle + \langle P_{\mu\nu,\mu\theta} \rangle + \langle P_{\phi} \rangle$$

Where,

$$\langle P_{\mu\nu} \rangle = \langle -\pi a^2 \rho \int_0^\pi \left(\frac{\partial \phi_1}{\partial v} \right)_{v=a}^2 \sin \theta \cos \theta d\theta \rangle$$

$$\langle P_{\mu\theta} \rangle = \langle \pi \rho \int_0^\pi \left(\frac{\partial \phi_1}{\partial \theta} \right)_{v=a}^2 \sin \theta \cos \theta d\theta \rangle$$

$$\langle P_{\mu\nu, \mu\theta} \rangle = \langle 2\pi a \lambda \rho \int_0^\pi \left(\frac{\partial \phi_1}{\partial v} \right)_{v=a} \left(\frac{\partial \phi_1}{\partial \theta} \right)_{v=a} \sin^2 \theta d\theta \rangle$$

$$\langle P_\phi \rangle = \langle -\frac{\pi a^2 \rho}{c^2} \int_0^\pi (\phi_1)_{v=a}^2 \sin \theta \cos \theta d\theta \rangle$$

For the radiation pressure on a compressible sphere, there are boundary conditions:

$$\frac{\partial \phi_1}{\partial v} = \frac{\partial \phi_2}{\partial v}, v = a$$

$$\rho \phi_1 = \rho \phi_2, v = a$$

$$\rho \frac{\partial \phi_1}{\partial \theta} = \rho \frac{\partial \phi_2}{\partial \theta}, v = a$$

Then $\langle P_{\mu\nu} \rangle, \langle P_{\mu\theta} \rangle, \langle P_{\mu\nu, \mu\theta} \rangle, \langle P_\phi \rangle$ can be expressed in term of ϕ_2 with the substitution $\cos \theta = \mu$:

$$\langle P_{\mu\nu} \rangle = \langle -\pi a^2 \rho \int_{-1}^1 \left(\frac{\partial \phi_2}{\partial v} \right)_{v=a}^2 \mu d\mu \rangle$$

$$\langle P_{\mu\theta} \rangle = \langle \pi \lambda^2 \rho \int_{-1}^1 \left(\frac{\partial \phi_2}{\partial \mu} \right)_{v=a}^2 \mu (1 - \mu^2) d\mu \rangle$$

$$\langle P_{\mu\nu, \mu\theta} \rangle = \langle -2\pi a \lambda \rho \int_{-1}^1 \left(\frac{\partial \phi_2}{\partial v} \right)_{v=a} \left(\frac{\partial \phi_2}{\partial \mu} \right)_{v=a} \mu (1 - \mu^2) d\mu \rangle$$

$$\langle P_\phi \rangle = \langle -\frac{\pi a^2 \lambda^2 \rho}{c^2} \int_{-1}^1 (\phi_2)_{v=a}^2 \mu d\mu \rangle$$

In a standing wave, ϕ_2 can be calculated as:

$$\phi_2 = \frac{1}{2}A[e^{-ik(z+x)} + e^{ik(z+x)}] = A \sum_{n=0}^{\infty} (2n+1) \cos(kh + \frac{1}{2}) \Psi(kr)(kr)^n P_n(\cos \theta)$$

Where x is the distance from a pressure node, $\Psi(kr)(kr)^n$ is the spherical Bessel function of order n and P_n is the Legendre function of order n.

Then we can calculate that the acoustic force as:

$$F_r = -\frac{4}{3}\pi\rho(ka)^3 A^2 \Phi(\beta, \rho) \sin(2kx) = -\frac{8\pi^2}{3\lambda} a^3 E \Phi(\beta, \rho) \sin(2kx)$$

$$E = \rho k^2 A^2$$

$$\Phi = \frac{5\rho_p - 2\rho_m}{2\rho_p + \rho_m} - \frac{\beta_p}{\beta_m}$$

Where E is the energy density, which can also be expressed as:

$$E = \frac{p^2}{Zc} = \frac{p^2}{\rho c^2} = p^2 \beta_m = \frac{p_0^2 \beta_m}{4}$$

Then acoustic force can be expressed as:

$$F_r = -\frac{8\pi^2}{3\lambda} a^3 E \Phi(\beta, \rho) \sin(2kx) = -\frac{8\pi^2}{3\lambda} a^3 \frac{p_0^2 \beta_m}{4} \Phi(\beta, \rho) \sin(2kx)$$

$$F_r = -\left(\frac{4\pi}{3\lambda} a^3\right) \frac{2\pi p_0^2 \beta_m}{4} \Phi(\beta, \rho) \sin(2kx) = -\left(\frac{\pi p_0^2 V_p \beta_m}{2\lambda}\right) \Phi(\beta, \rho) \sin(2kx)$$

As a result, in SSAW, the primary acoustic force (F_r) and the viscous force (F_v) on a particle show as follows [22, 40, 43, 44]:

$$F_r = -\left(\frac{\pi p_0^2 V_p \beta_m}{2\lambda}\right) \Phi(\beta, \rho) \sin(2kx)$$

$$\Phi = \frac{5\rho_p - 2\rho_m}{2\rho_p + \rho_m} - \frac{\beta_p}{\beta_m}$$

$$F_v = -6\pi\eta r v_h$$

Where p_0 , V_p , λ , k , x , ρ_m , ρ_p , β_m , β_p , η , d and v_h correspond to pressure amplitude, particle volume, ultrasonic wavelength, wave vector, distance from a pressure node, density of the medium, density of particles, compressibility of medium, compressibility of particles, medium viscosity, particle diameter, and relative velocity, respectively.

For SAW device driving by piezoelectric ceramics, p_0 can be calculate:

$$p_0 = \sqrt{\frac{PZ}{A}}$$

Where $Z = \rho \cdot c$, is the acoustic impedance, and $\rho = 4650 \text{ kg} \cdot \text{m}^{-3}$, $c = 3900 \text{ m} \cdot \text{s}^{-1}$ are the density and SAW velocity of the LiNbO_3 substrate, respectively. A is the SAW working area, and P is the input power.

At the stable point (pressure node or anti-pressure node), the acoustic force and viscous force will balance each other.

$$F_r = F_v$$

Since the particles will move to the pressure nodes nearby, the x is the displacement from a pressure node with a range from 0 to wavelength/4. Therefore the time needed for bead migration will be:

$$v_h = -\frac{p_0^2 V_p \beta_m}{12 \lambda \eta r} \Phi(\beta, \rho) \sin(2kx)$$

Rewriting $v_h = -dx/dt$, we can get:

$$\csc(2kx) dx = \frac{p_0^2 V_p \beta_m}{12 \lambda \eta r} \Phi(\beta, \rho) dt$$

$$t = \frac{\left(\frac{3\lambda^2 \eta d}{2\pi}\right) \left\{ \ln \left[\tan \left(\frac{2\pi x}{\lambda} \right) \right] \right\}_{x_1}^{x_2}}{\pi p_0^2 V_p \beta_m \Phi(\beta, \rho)}$$

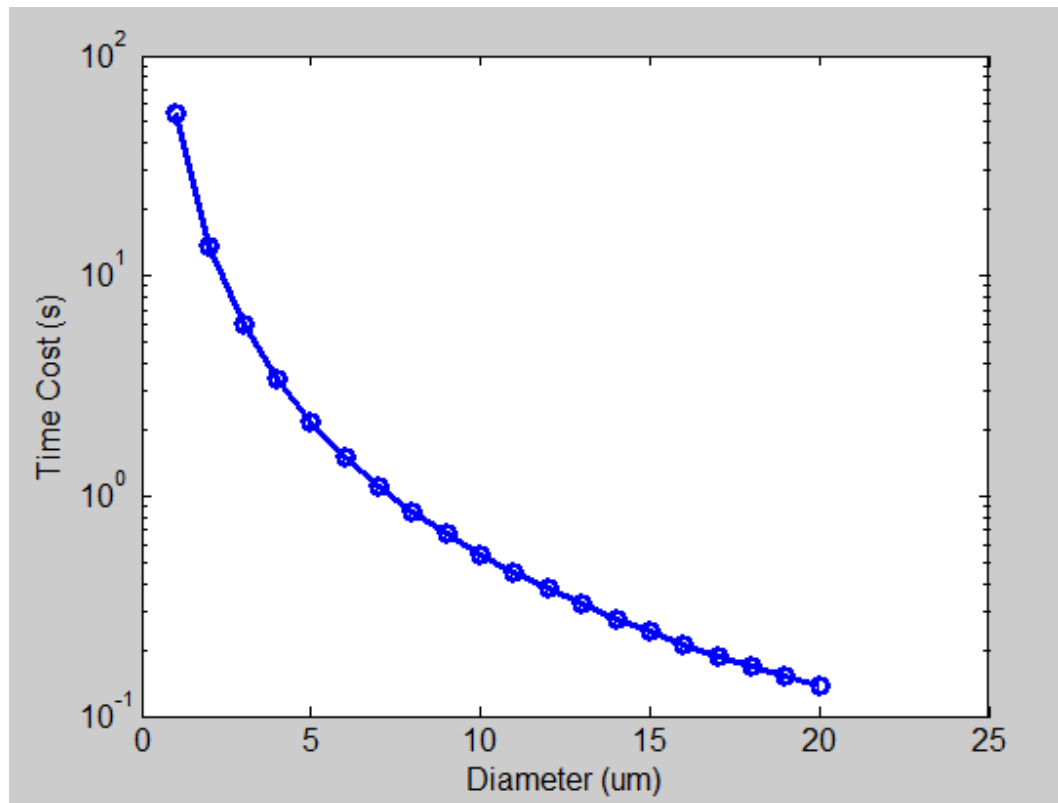


Figure 3-3 Relationship between particle size and time cost. It shows the time of different sizes of polystyrene beads move from anti-pressure node to pressure node in the water in a designed SSAW with fixed applied voltage on the IDTs. The range of particle diameter is from 1 μm to 20 μm . Wavelength is 400 μm and applied voltage is 14 V_{P-P} .

From the formula above, we can get the figure that shows the relationship between diameter of particle and the time cost. (Figure 3-3) Within a fixed time, bigger particles travel a larger lateral displacement than the smaller ones. Therefore by adjusting the flow velocity, channel length and SAW power, particles with different size travel different distances in the width direction of the microchannel; the particles are hence separated.

3.2 Design Plans

This separation device is designed with two stages. The first one is the focusing stage that all particles are focused in one line at the pressure node of SSAW generated by the pair of IDTs at the first stage. The second stage is the particle separation stage. The designed position of pressure node of SSAW field at the second stage is different from the pressure node of SSAW field generated at the first stage.

Under the function of SSAW field, all different size particles will move from the pressure node of SSAW field at the first stage to the new pressure node of SSAW field at the second stage, with a different speed depends on different particle size. Within the same time, the bigger the particles size is, the greater and the faster they will move. Therefore, the particles can be separated. Three types of design are presented, compared and analyzed as follows.

3.2.1 Option one

As shown in Figure 3-4, the red lines within the channel of both stages are the pressure nodes of SSAW field. Under the action of SSAW field at the first stage, all the particles at the first stage are concentrated on the pressure node in the middle of the channel. When they move into the second stage, the middle of the channel is changed to the anti-pressure node of the second stage; the particles will move to the new pressure nodes at the second stage. In this design, IDTs at first stage and second stage are designed with same wavelength.

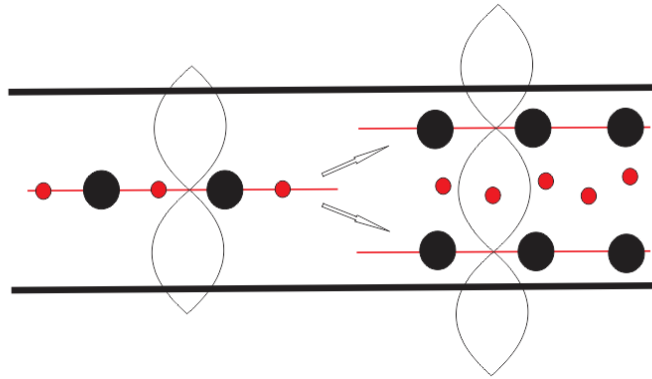


Figure 3-4 Scheme of design option one

This design is workable but there are some problems. Although particles will move from the anti-pressure node to the pressure node in the SSAW field, but the force at exactly the anti-pressure node is zero. As a result, in the beginning of the second stage in this design, the particles are at the metastable position, so some particles may keep in this position and do not move to the new pressure nodes. The separation may be incomplete.

3.2.2 Option two

In the second design, all particles are firstly focused in two different lines at the focusing stage. Then they will move to the new pressure node line at the separation stage which is designed in the central of the channel. The wavelength of separation stage is designed as two times as the wavelength at the focusing stage.

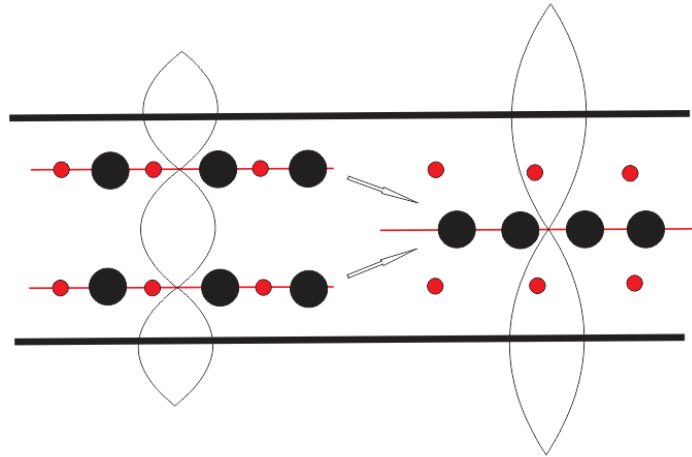


Figure 3-5 Scheme of design plan two

This design avoids the anti-pressure node by using different wavelength at the different stages. But the gaps of IDTs at the first stage are too small, which increase the difficulty in fabrication. Moreover a perfect bonding was required; any tilt of microchannel may result in the failure of separation. (Figure 3-6)

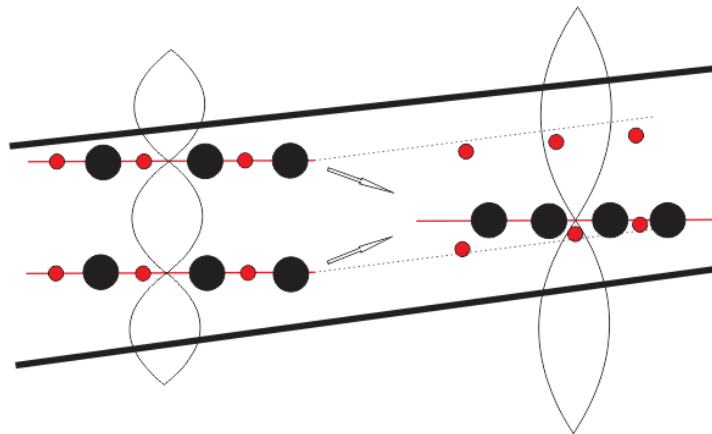


Figure 3-6 Scheme of tilted design option two, particles may not be separated

3.2.3 Option three

In this design, the particles are focused in one line at the first stage as shown in Figure 3-7. The position of IDTs at the second stage shifts to the left to another line compared to the IDTs at the first stage. As the position of IDTs is changed, the position of pressure node and anti-pressure node of SSAW generated at the different stage will be changed as well.

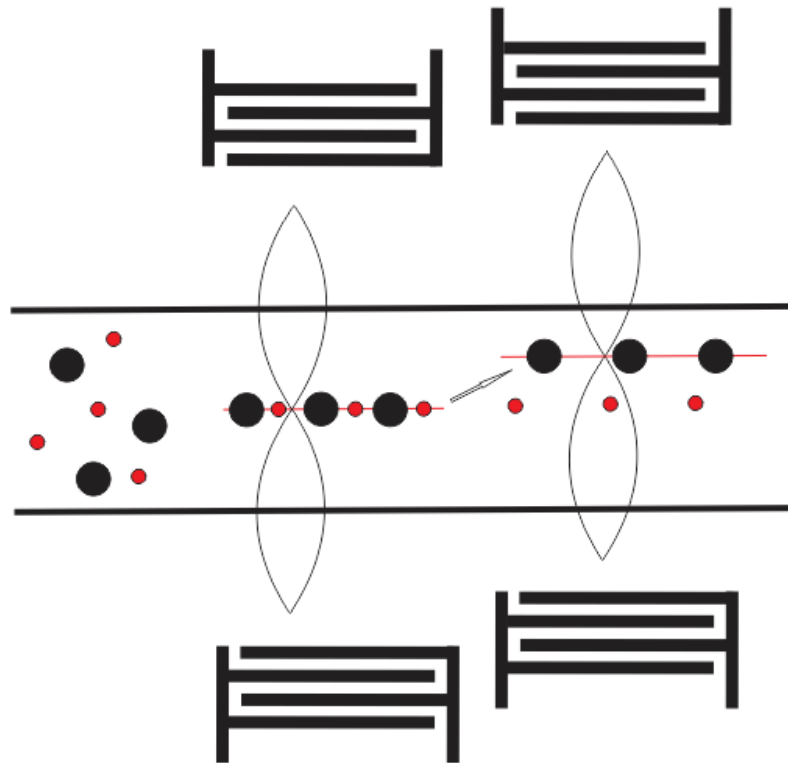


Figure 3-7 Scheme of design option three

This design avoids using the anti-pressure node. The offset of pressure node at the second stage can be controlled to the left or to the right compared to the first stage by changing the junction order of connection wires. As a result, if the microchannel is tilt, we can adjust the position of pressure node of the

second stage to get good separation result. This design is adopted as the final design for it is easy to fabricate, bond and adjustable. Moreover it is suitable to be extended to a wide channel design to increase the throughput.

By applying a high voltage at the first stage, all the particles will move to the pressure node line quickly, and be focused in one line before the ending of stage one. Then we apply a lower voltage on the second stage IDTs, the bigger particles are driven to the new pressure node quickly, while the smaller one will have a much shorter movement along the SAW propagation direction. Hence the two sizes of particles are separated successfully.

3.3 Calculation

Some parameters which will be used in the calculation are found in the Wikipedia and lists in the table 3-1. The viscosity of water is 1.02×10^{-3} .

Polystyrene beads with different size, 20 μm and 5 μm , are used in the calculation and experiments.

	Density(ρ)(kg/m^3)	β	$\Phi(\beta, \rho)$
Polystyrene (particle)	1050	1.56×10^{-10}	0.76
DI Water (medium)	980	5.1×10^{-10}	

Table 3-1 Parameter of polystyrene beads (particle) and DI water (medium)

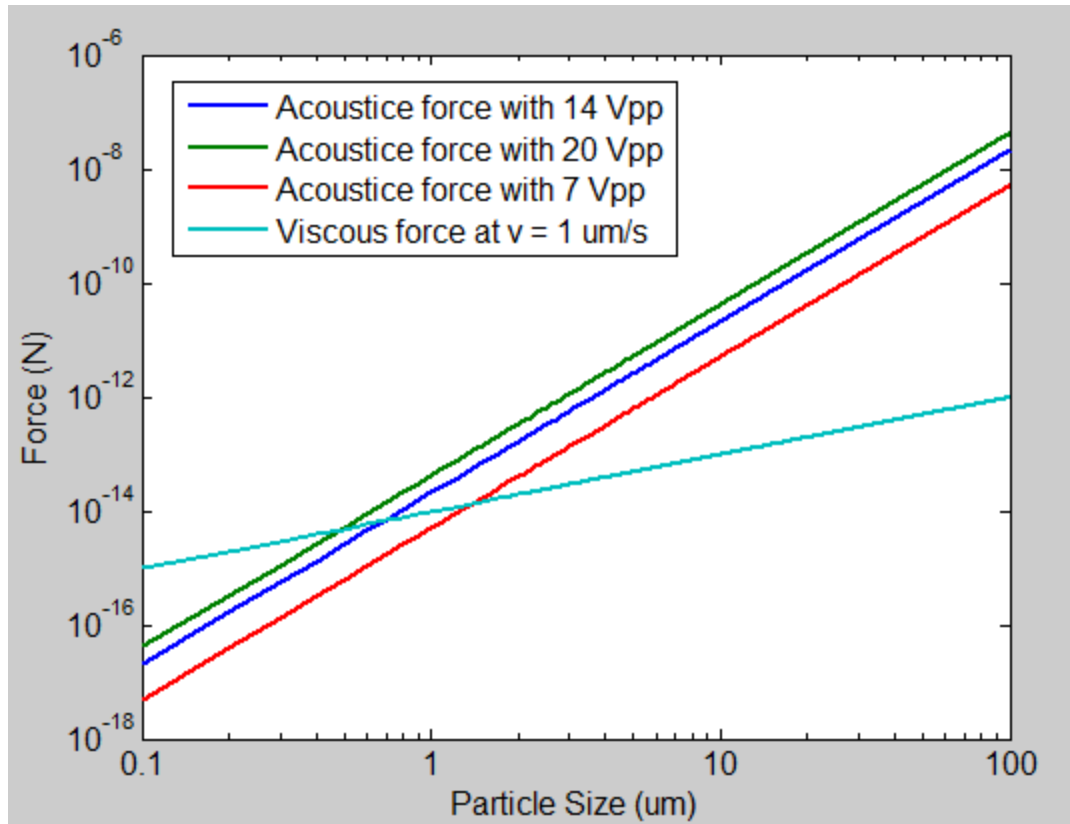


Figure 3-8 Forces of particle in SSAW field. Particles can move only when acoustic force is bigger than viscous force. Acoustic force can be increased by increasing the particle size or applying a higher voltage. Wavelength is 400 μm .

Forces applied on particles in SSAW field can be calculated by the equations listed in Chapter 3.1. The acoustic force applied on 20 μm polystyrene beads is 165.7 pN, while that applied on 5 μm polystyrene beads is only 2.6 pN, with a difference of 64 times. The difference of viscous force, which is proportional to the radius of the particles, is not so big, just 4 times different. As a result, the bigger particles will move much faster than the smaller one. The gravity and buoyancy balanced each other and can be ignored in the calculation.

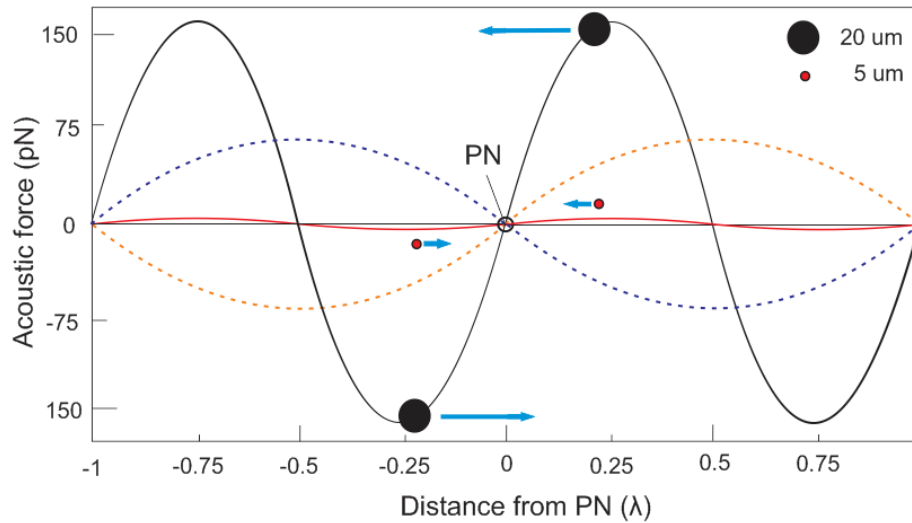


Figure 3-9 Acoustic forces applied on different parities in SSAW field

As shown in Figure 3-9, the acoustic force distribution along a SSAW wavelength follows sinusoid; with a distance of $1/8$ wavelength to the pressure node, applied force on particles generated by SSAW field reaches to the maximum value. In order to get the minimum separation time and save the input power at the separation stage, the offset between the first stage and the second stage is set to $1/8$ wavelength of SAW. Also, the smaller wavelength it is, the bigger the acoustic force will be. For separating $20\ \mu\text{m}$ and $5\ \mu\text{m}$ mixed polystyrene particles, this offset and wavelength cannot be small. So the wavelength of SAW is designed as $400\ \mu\text{m}$, while the offset is $50\ \mu\text{m}$ which is big enough for the separation.

➤ At the first stage, input voltage is set to $20\ V_{P-P}$, while input power is 1W ; if the input voltage is $14\ V_{P-P}$, input power will be $500\ \text{mW}$; working area is $3.5 \times 10^{-4}\text{m}^2$.

The initial position and the balanced position, which is near the pressure node of the SSAW, are defined as $x_1 = \frac{\lambda}{40}$, $x_2 = \frac{9\lambda}{40}$, respectively. Then the need time t for congregating is calculated.

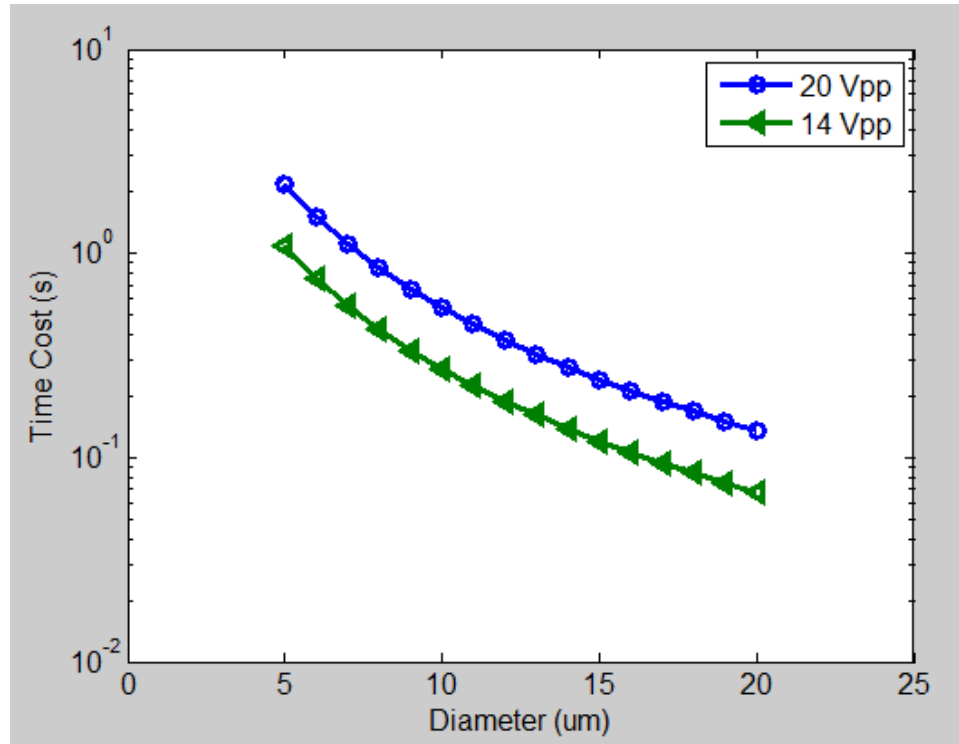


Figure 3-10 Focusing time with different applied voltage. Wavelength is 400 μm .

Voltage (V_{P-P})	Power (mW)	Focusing time (s)	
		20 μm	5 μm
20	1000	0.07	1.09
14	500	0.13	2.18

Table 3-2 Calculated focusing time

As shown in Figure 3-10 and Table 3-2, two different size polystyrene beads can be focused on the pressure node in a short time.

➤ At the second stage, input voltage is set to $7 V_{P-P}$, while input power is 120 mW, working area= $3.5 \times 10^{-4} m^2$.

The initial position and the balanced position, which is near the pressure node of the SSAW, are defined as $x_1 = \frac{\lambda}{8}$, $x_2 = \frac{9\lambda}{40}$, respectively. The need time t for whole movement is calculated.

$$t_{\text{big}} = 0.28s, \quad t_{\text{small}} = 4.54s$$

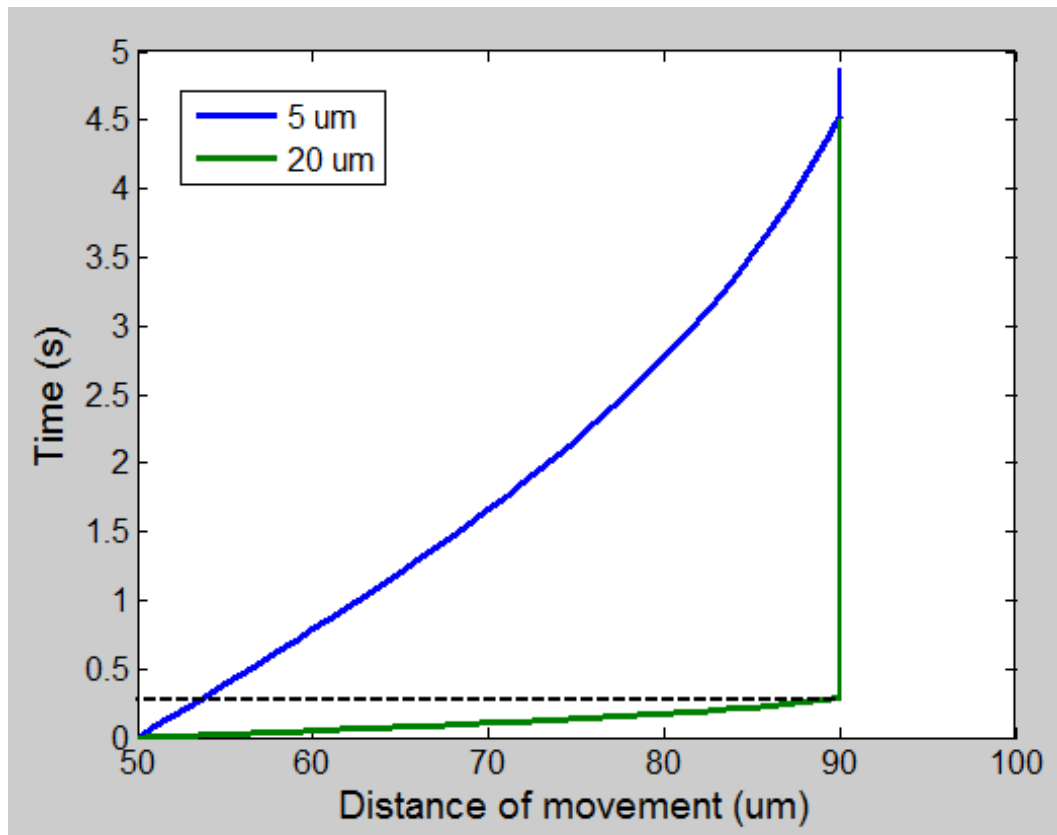


Figure 3-11 Calculated travel distance of 20 μm and 5 μm polystyrene beads. The dash line shows the difference of two particles' movement at 0.28s, which is about 36 μm . Wavelength is 400 μm and applied voltage is $7 V_{P-P}$.

At 0.28s, the 20 μm polystyrene beads are at the new pressure node line with a movement of 40 μm , while the 5 μm polystyrene beads just move less than 4 μm . Then these two size beads are separated successfully and we can collect them in different sub channels separately. (Figure 3-11)

3.4 Design of IDTs

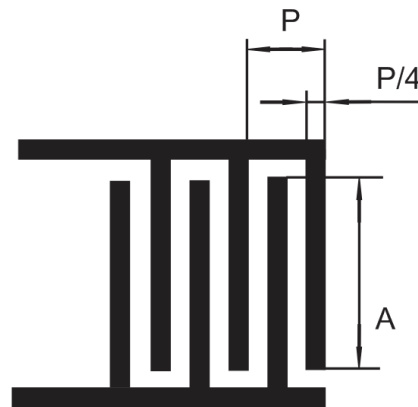


Figure 3-12 Schematic illustrations of IDT

The design of IDT is very mature, since it has been developed for several decades. As the wavelength of SSAW field of both stages are designed as 400 μm with 15 pairs of electrodes, the period, p , was 400 μm . The width of electrode and gap between electrodes are equal, designed as 100 μm .

According to the calculated focusing time at the first stage and separation time at the second stage, about 1s and 0.3s (Table 3-3), the apertures of IDTs at stage one and stage two are designed with a similar ratio as 7.2 mm and 2.5 mm, respectively.

Voltage (V_{P-P})	Power (mW)	Focusing time (s)	
		20 μm	5 μm
20	1000	0.07	1.09
Voltage (V_{P-P})	Power (mW)	Separating time (s)	
		20 μm	5 μm
7	120	0.28	4.54

Table 3-3 Calculated focusing and separation time of different applied voltage

3.5 Design of channel

The microchannel is designed as 180 μm in width and 90 μm in depth with one inlet/reservoir and two outlets/reservoirs so as to collect different particles.

Polydimethylsiloxan (PDMS), which chemical formula is $\text{CH}_3\text{-}[\text{Si}(\text{CH}_3)_2\text{O}]_n\text{-Si}(\text{CH}_3)_3$, is selected to be used for building the microchannel because of its low price, easy to fabricate and reusable of the mold. Another reason is as a polymer material, PDMS is optically clear, and considered to be inert, non-toxic and non-flammable.

We have also developed a new method to remove PDMS channel completely in a short time, so it is very convenient and safe to use PDMS as the microchannel, which will be shown in the Chapter 4.

3.6 Select of substrate

Lithium niobate (LiNbO_3) is one type of piezoelectric material and was original synthesized in 1965. LiNbO_3 is a compound of niobium, lithium, and oxygen. Its single crystals are an important material for optical waveguides,

optical modulators and surface acoustic wave substrate. This material is widely used to generate SAW. [21-32, 34-36, 40]

128° Y-rotated LiNbO₃ that can restrain the generation of Bulk acoustic wave (BAW) mostly is used in our device as the SAW substrate. A coating of a double metal layer (Au/Cr, 100 Å /1000 Å) is used to fabricate the electrodes. The back side of LiNbO₃ substrate is unpolished to suppress the generation of BAW.

CHAPTER IV

FABRICATION

Masks for the electrode and channel were designed by AutoCAD and printed from CAD/ART Services, Inc. Then the electrodes on the LiNbO₃ wafer and PDMS channels were fabricated separately and then bonded together using the oxygen plasma to finally get the particle separation device based on standing surface acoustic waves.

4. 1 Electrode fabrication

The electrodes were made on a gold coated LiNbO₃ substrate. The photo-resist of AZP4620 was used in the process of fabrication. We started the fabrication process with a 4-inch LiNbO₃ wafer.

Step 1) Cleaned the LiNbO₃ wafer with acetone, isopropanol alcohol or ethyl alcohol and distilled water. The wafer was dehydrated on a hot plate with a temperature of 100°C. (Figure 4-1 A)

Step 2) Deposited a thin film of photo-resist AZP4620 on the LiNbO₃ wafer by using Laurell WS-400B-6NPP/LITE spin-coater. (Figure 4-1 B)

Step 3) Did the soft bake on the hot plate, with 100°C for 1 min, 120°C for 1.5 min and 100°C for 1 min.

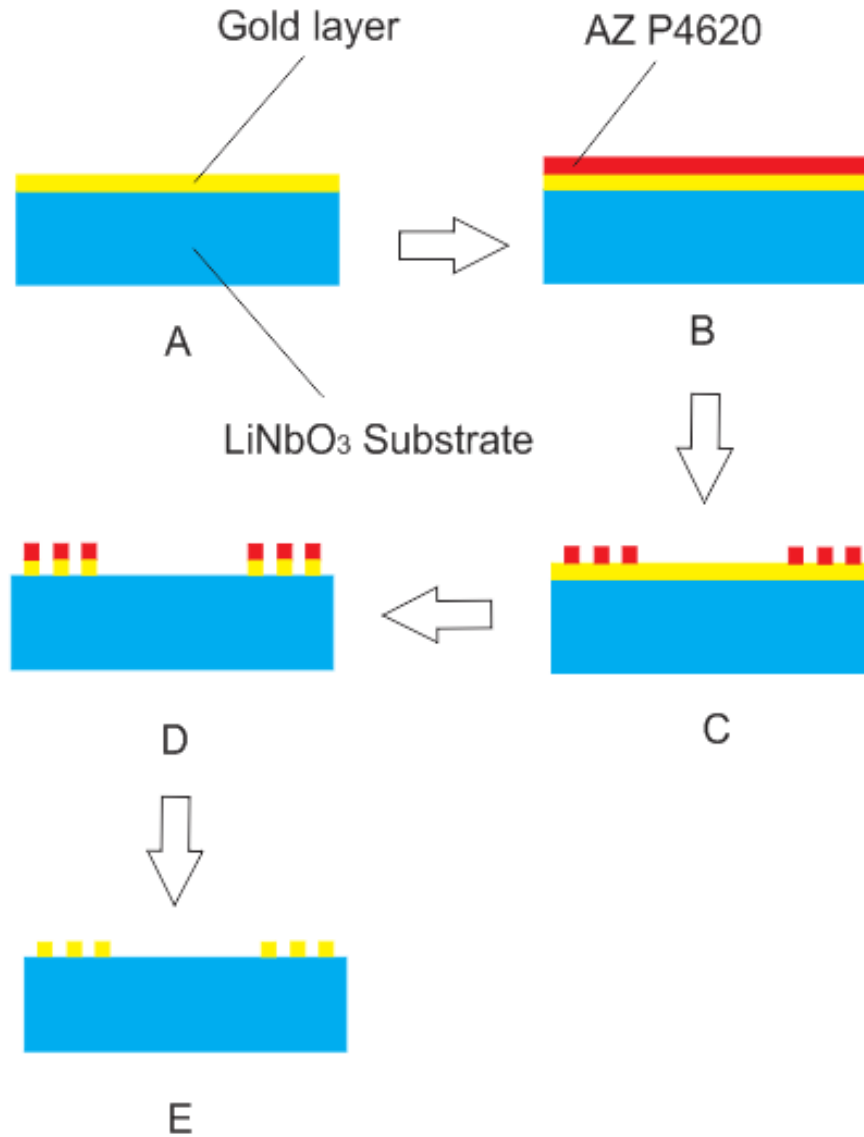


Figure 4-1 Process flow of fabricate electrodes on LiNbO_3 Substrate

Step 4) The wafer was then exposed to UV-light for 18 sec through the electrode mask to transfer the pattern on the mask to the photo-resist layer, by using OAI 206 UV mask aligner. Being a positive photo-resist, the exposed areas became more soluble in the developer solution than the non-exposed areas. (Figure 4-1 C)

Step 5) The wafer was developed in AZ developer AZ 400K to remove the non-exposed parts of the resist. Then the pattern could be seen. After observed with Mitutoyo FS70 high precision microscope, did the hard bake at 100°C for an hour.

Step 6) Therefore, the wafer was etched with gold etchant and chromium etchant carefully to remove the gold and chromium layers on the wafer which are not covered with photo-resist. (Figure 4-1 D)

Step 7) Cut the 4-inch LiNbO₃ wafer into designed devices using the wafer cutter machine Sherline 5410 slowly. LiNbO₃ wafer is very fragile, so high cutting speed or high amount of feed is not allowed.

Step 8) Finally, removed the remained photo-resist over the remaining part of the gold by immersing the device in the AZ stripper AZ 400T solution for a long time. (Figure 4-1 E)

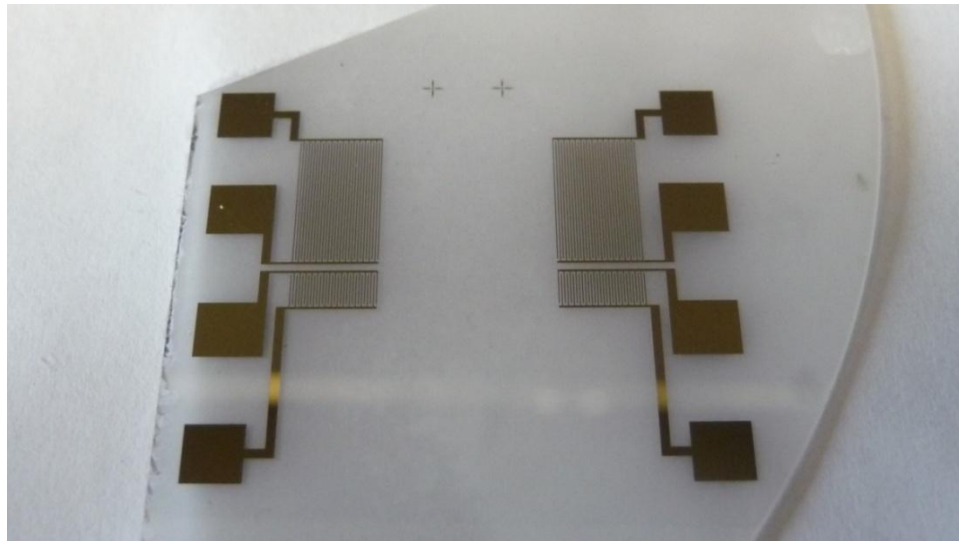


Figure4-2 Picture of microfabricated electrode of particle separation device based on SAW. Two pairs of IDTs are fabricated on LiNbO₃ substrate.

4.2 Channel fabrication

The channel fabrication has two separated steps. Firstly it was fabricated to make a mold of the channel on glass substrate. Then PDMS solution was poured over the glass substrate which, when cured, formed the designed channel.

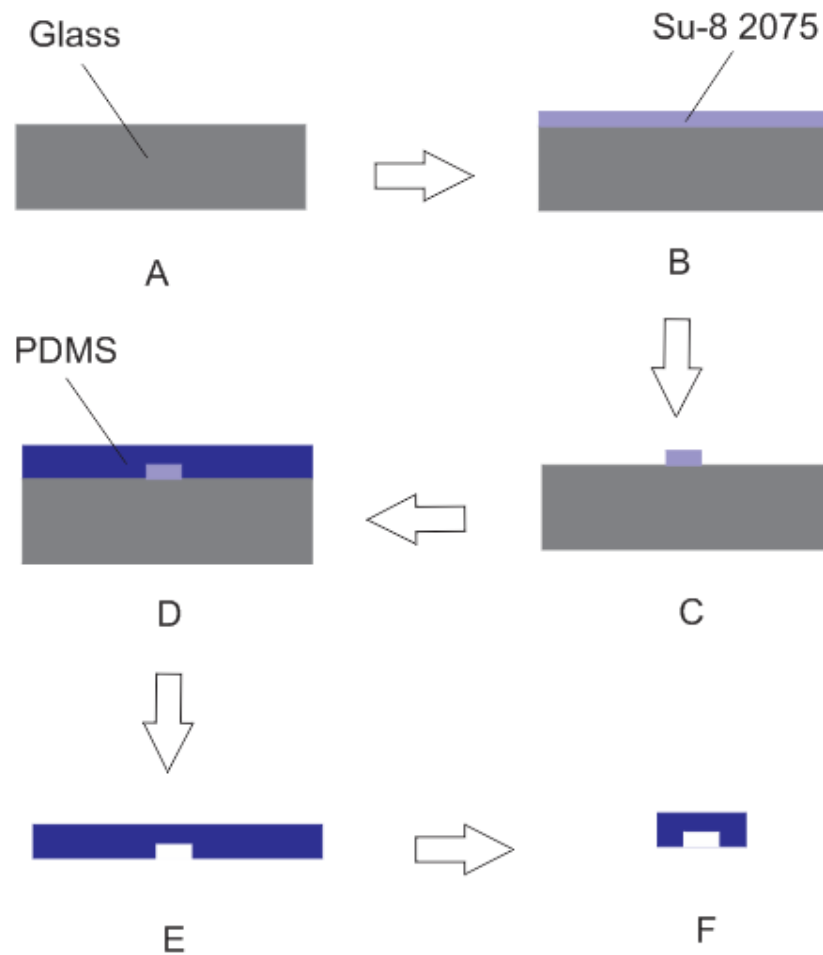


Figure 4-3 Process flow of making a PDMS channel

4.2.1 Mold fabrication

The electrodes were made on a glass substrate. The photo-resist used in this fabrication process was SU8 2075.

Step1) Cleaned glass substrate for about 10 minutes in an ultrasound water bath and then rinsed with acetone, isopropanol alcohol or ethyl alcohol and distilled water. Then put the wafer on a hot plate with a temperature of 100°C to do dehydration. (Figure 4-3 A)

Step 2) Deposited a thin film of photo-resist SU8 2075 with a thickness of 90 μm on the glass substrate by using Laurell WS-400B-6NPP/LITE spin-coater, while the spin speed was optimized to 2000 rpm. (Figure 4-3 B)

Step 3) Did the soft bake on the hot plate, with 65°C for 10 min, 80°C for 40 min. Although the recommend temperature is 65°C and 95°C, SU8 film may become unfairness at 95°C on our hot plate. That may be the result of the uneven heating of our hot plate. So I chose 80°C to get a fairness film.

Step 4) Glass substrate was then exposed to UV-light for 27 sec through the electrode mask to transfer the pattern on the mask to the photo-resist layer, by using OAI 206 UV mask aligner. A filter was kept in between the light ray and the mask to get a clear boundary of the design on the SU-8. Being a negative photo resist, the non-exposed areas became more soluble in the developer solution than the exposed areas.

Step 5) Did the post-exposure on the hot plate, with 65°C for 5 min and 80°C for 15 min. Then the pattern could be seen.

Step 6) The glass substrate was then developed in SU8 developer to remove the non-exposed parts of the resist. By flushing IPA on the SU8 film, we can check whether it is still underdeveloped or not. After observed with Mitutoyo FS70 high precision microscope, did the hard bake at 100°C for an hour. (Figure

4-3 C)

Step 7) For SU8 mold, it can be measured with Veeco Dektak 150 profilometer, then the dimensions of height and width of the mold will be checked. The mode we got is 180 μm in width and 90 μm in depth, which is exactly the same as we designed. (Figure 4-3 D)

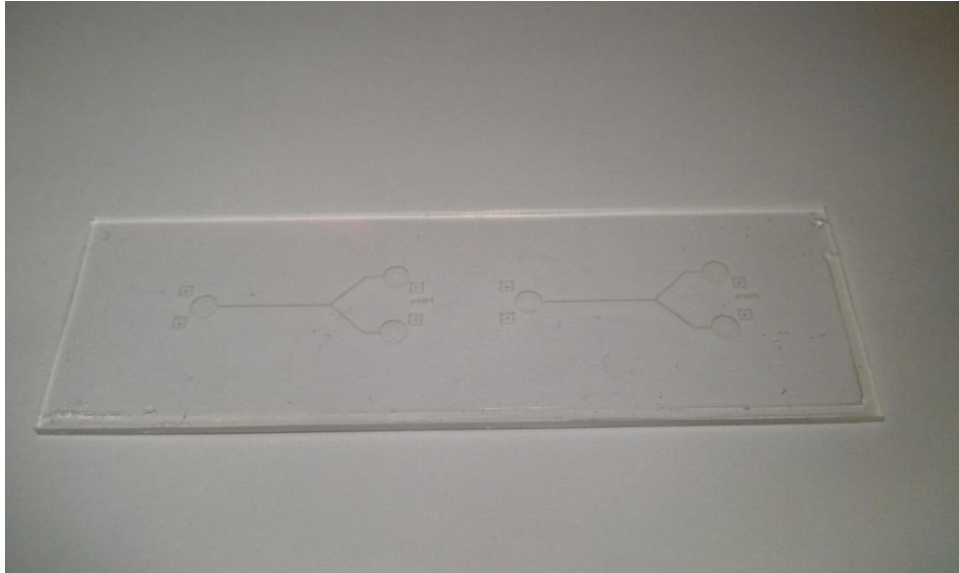


Figure 4-4 Photo of channel mode fabricated on a glass substrate

4.2.2 PDMS channel

The first step of making PDMS was to mix and stir the silicone elastomer and the curing agent sufficiently with a ratio of 10:1. This mixed liquid was then poured over the SU-8 mold placed in an aluminum-foil paper container. The PDMS was vacuumized to remove air bubble and then cured in an oven for about 12 hours at 60 $^{\circ}\text{C}$.

Then the cured PDMS could be peeled off from the mold and cut off the boundary carefully. At last, holes of the inlet and outlet reservoirs will be drilled; it

should be cleaned up for future use. (Figure 4-3 E and F)

4.3 Channel and electrode bonding

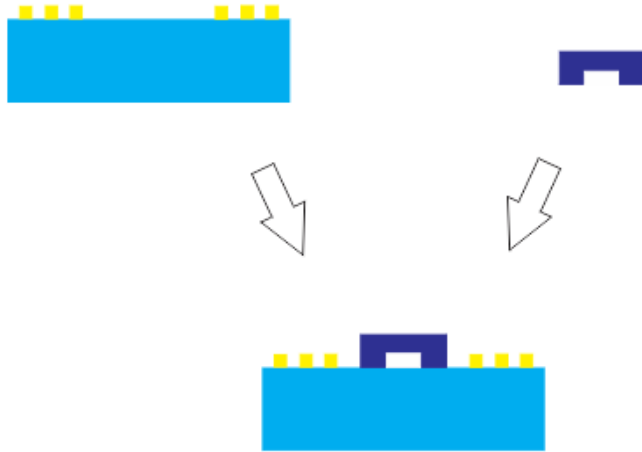


Figure 4-5 Bonding of LiNbO₃ substrate and PDMS channel

LiNbO₃ wafer with electrode on it and the microchannel we made were both put in the oxygen plasma bonder, Plasma cleaner PDC- 32G, and then they were exposed for 40 seconds. After that, PDMS channel and electrode were aligned with designed align marks under the microscope. During the alignment, a solution of methanol and water with a ratio of 2:1 was used to prevent them from sticking together immediately. (Figure 4-5)

After that we heated the combined device on a hot plate, increasing temperature to 150°C gradually, then the bonding would be done after several hours. If this kind of bonding is between the PDMS and glass substrate, a lower temperature and shorter heating time will be applied.

The connection wires were bonded to the electrode with conductive glue,

silver Conductive Epoxy 8331, which has a good conductivity and can be removed under a low temperature or immersed in the organic solvents such as IPA, ethyl alcohol or AZ stripper etc. In our experiment, AZ stripper was preferred because it takes a much shorter time than IPA and ethyl alcohol.



Figure 4-6 Plasma cleaner PDC- 32G equipped with vacuum pump

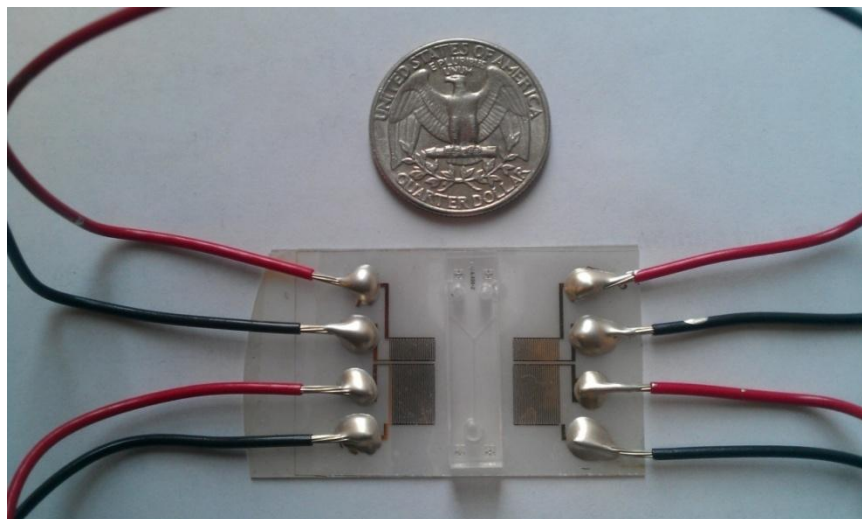


Figure 4-7 A picture of the completed particle separation device with bonded connection wires.

4.4 Removal of PDMS

The bonding of PDMS to substrates such as glass, LiNbO₃ etc. was considered to be irreversible. Actually it really takes a long time to dissolve PDMS completely; dissolving PDMS with a thickness of 5mm will take several months.

Solvent	Swelling Ratio
diisopropylamine	2.13
triethylamine	1.58
chloroform	1.39
ether	1.38
benzene	1.28
ethyl alcohol (ethanol)	1.40

Table 4-1 Swelling Ratio of PDMS in major organic solvent,

Copy from <http://neubrandinc.com/blog/category/pdms/>

Besides dissolving PDMS, organic solvents can also swell PDMS. The bonding of PDMS to the substrate can be broken up by a huge swelling of PDMS channel. In our experiment, ethyl alcohol was chosen because it is not harmful to human being and has a good swelling ratio so that it can break up the bonding in a short time. PDMS channel can be easily peeled off from LiNbO₃ substrate completely after 3 days immersed in ethyl alcohol. It will not harm or etch the electrode and substrate. And the bonded connection wires can also be removed simultaneously.

CHAPTER V

EXPERIMENTAL RESULT AND ANALYSIS

5.1 Experimental units

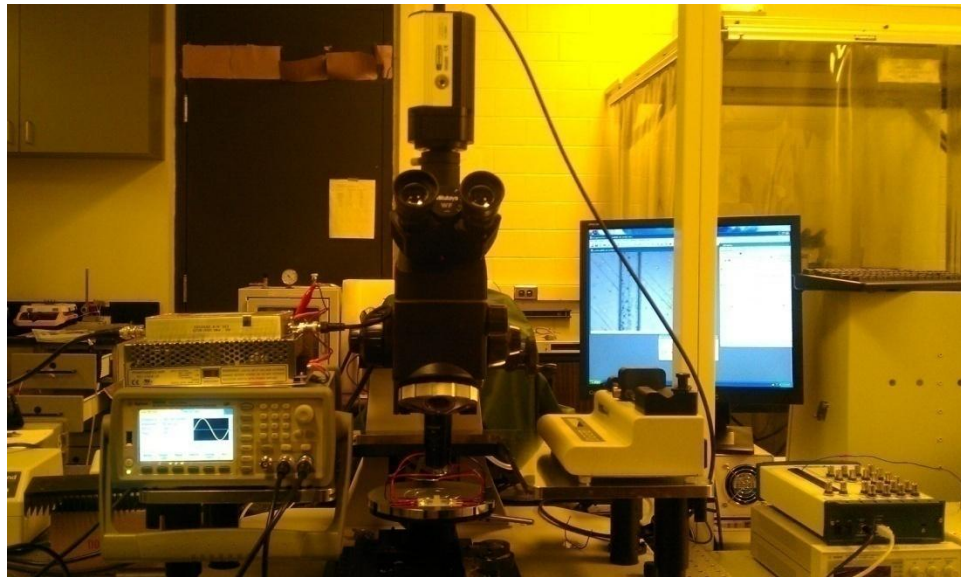


Figure 5-1 The photo of experimental Units

In our experiment, particles suspended in DI water were pumped into the PDMS microchannel by using a KDS-100 syringe pump with adjustable flow rate. A two-channel function generator (Agilent 33522A) was used to generate RF signals. RF signals generated in one channel was amplified to a higher magnitude by an OPHIR RF 5302032 amplifier and applied to the IDTs at the first stage. The RF signal induced a SSAW field to focus all suspended particles; the

RF signal from the other channel was applied to the second stage IDTs directly without amplification, which generated a relatively weaker SSAW field to separate different size particles. We observed and recorded the particle traces by a Mitutoyo FS70 high precision microscope equipped with a high resolution camera (QI-CAM, Qimaging).

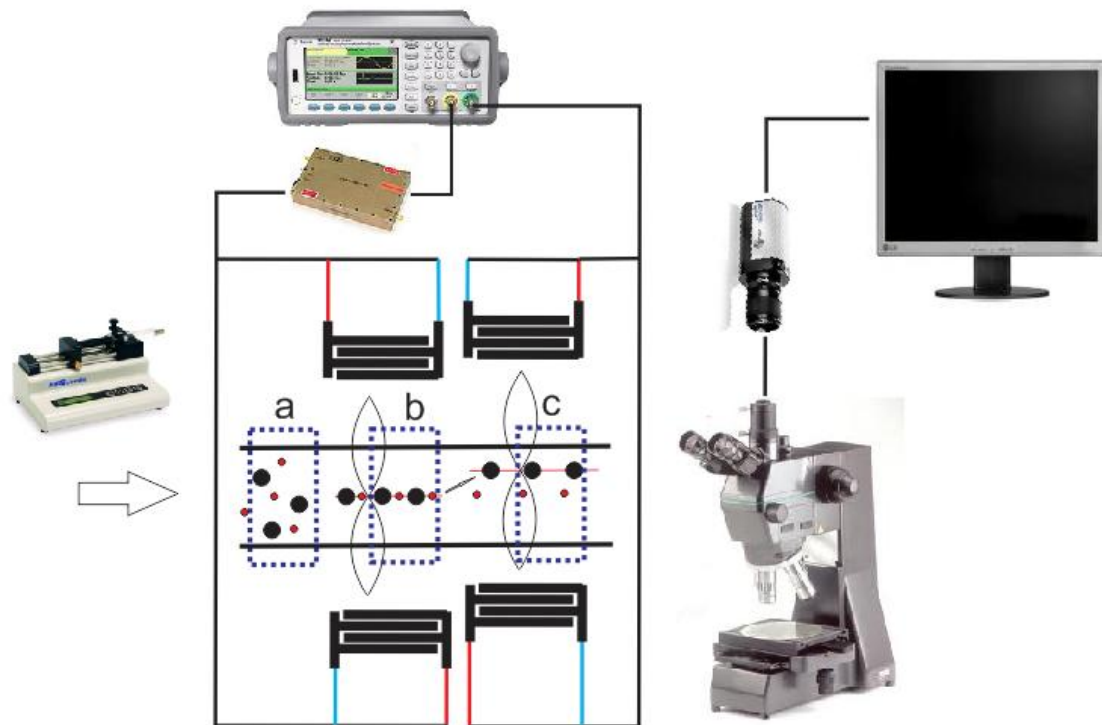


Figure 5-2 Experimental setup for the particle separation device, particle traces at three positions (a, b, c) were recorded by CCD camera and analyzed.

5.2 Preparation of experimental sample

Two different sizes of particles, 20 μm polystyrene beads solution (with 1% concentration) and 5 μm polystyrene beads solution (with 1% concentration)

were mixed with a ratio of 4:1. Then the mixed particle solution was diluted 20 times. Surfactant Triton-X-100 was used to reduce the particles aggregation.

5.3 Experimental results

In our experiments, particle solution containing 20 μm and 5 μm mixed polystyrene beads, was introduced in the microchannel with a width of 180 μm by using a syringe pump KDS-100. The throughput we set was 50 $\mu\text{L}/\text{hour}$, thus the velocity of inlet flow was 860 $\mu\text{m}/\text{s}$.

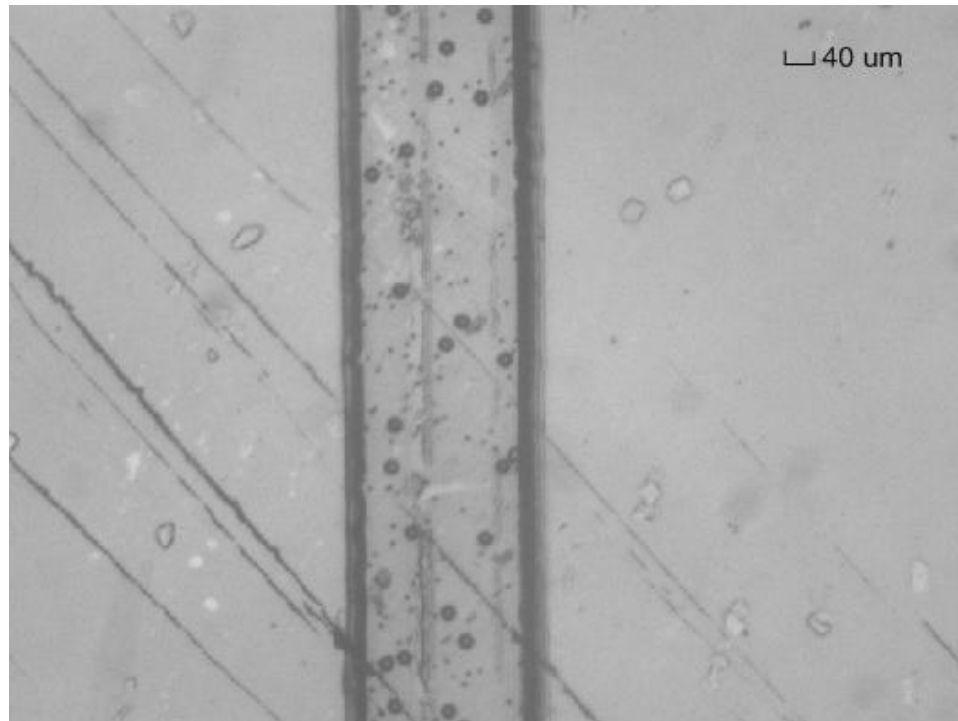
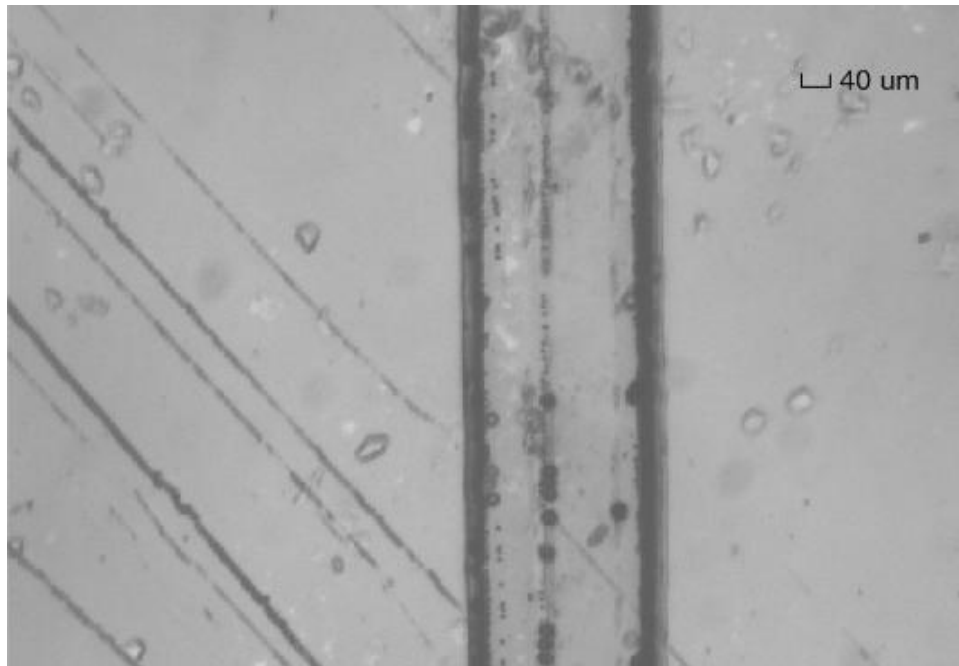


Figure 5-3 Mixed particles were inducted into microchannel at position **a** of Figure 5-2; flow rate was set to be 50 $\mu\text{L}/\text{hour}$.

As shown in Figure 5-4, at the first stage, because of the strong acoustic fields and the larger acoustic forces on particles, all particles were focused on the pressure node of SSAW field with a voltage of 20 V_{P-P} applied on the first pair of IDTs. At the second stage, the position of pressure node was shifted to another line with 50 μm offset to the left. When a voltage of 7 V_{P-P} was applied on the second stage IDTs, all the 20 μm beads were driven to the new pressure node in 0.3 sec; while the 5 μm beads, did not exhibit an obvious movement along the SAW propagation direction at the same time. This is because the weaker acoustic field and smaller acoustic forces applied on the particles. Figure 5-5 shows that the two size beads were separated with a distance of 36.5 μm. Note that in this experiment, the frequency of applied RF signal was optimized to 9.48 MHz to get the best result.



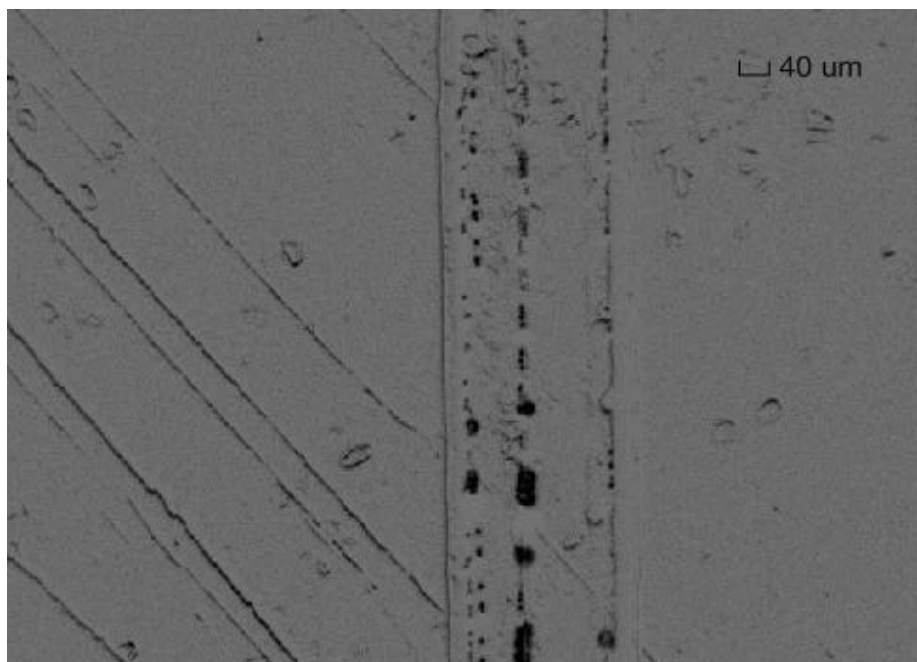
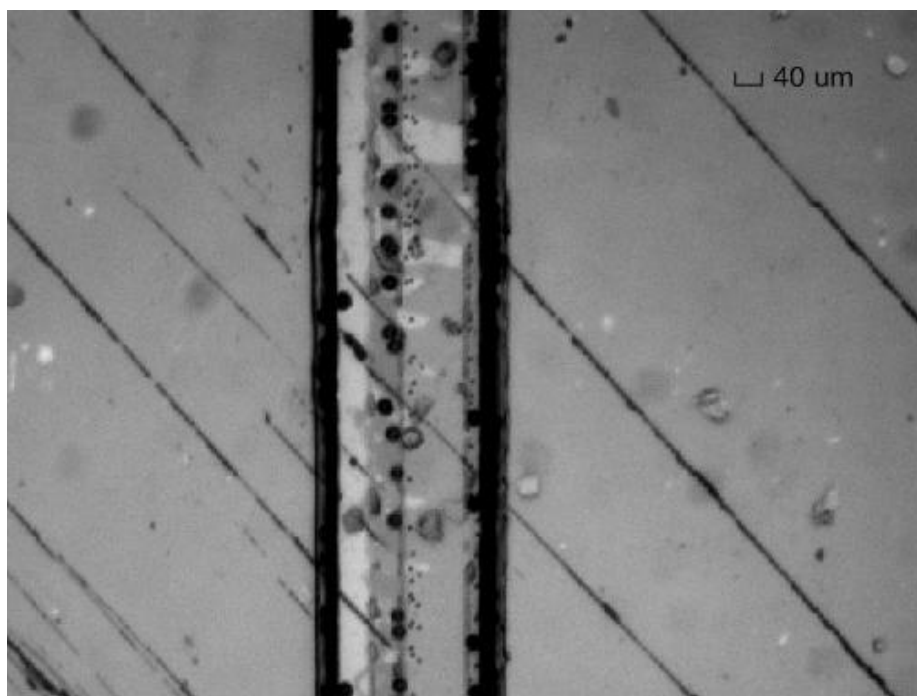


Figure 5-4 Particles were focused in a line at the first stage at position **b** of Figure 3-2; flow rate was set to be 50 $\mu\text{L}/\text{hour}$, frequency was 9.48 MHz, applied voltage was 20 $V_{\text{P-P}}$.



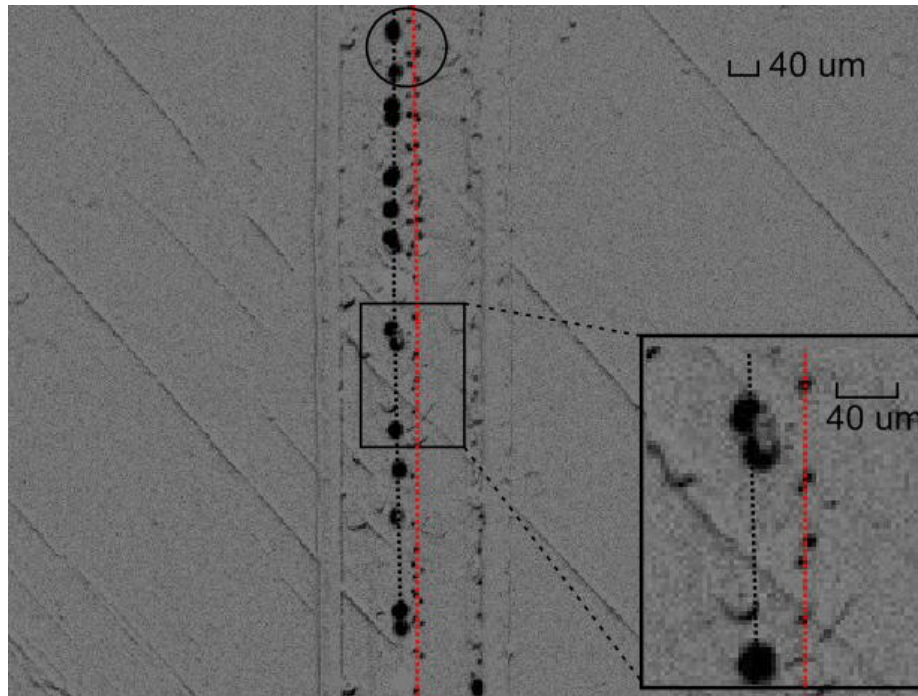


Figure 5-5 Two types of beads were separated into two lines at the second stage at position **c** of Figure 3-2. The distance between the two lines reaches the maximum value in the rectangular box which is approximately $36.5\ \mu\text{m}$. The distance between the two lines in the circle area is approximately $27.8\ \mu\text{m}$. The distance between two analyzed positions in the rectangular box and circle area is $440\ \mu\text{m}$. The applied voltage was $7\ \text{V}_{\text{P-P}}$, frequency was $9.48\ \text{MHz}$, The flow rate was set to be $50\ \mu\text{L}/\text{hour}$, thus the velocity of inlet flow was $860\ \mu\text{m}/\text{s}$.

The predicted maximum distance of $20\ \mu\text{m}$ and $5\ \mu\text{m}$ beads from calculation was $36.4\ \mu\text{m}$ at $0.28\ \text{sec}$ ($90\ \mu\text{m} - 53.6\ \mu\text{m}$); while the picture obtained from the CCD camera showed that the real distance of two lines is $36.5\ \mu\text{m}$. The distance between two different analyzed position is $440\ \mu\text{m}$, so travel

time is about 510ms. The predicted distance of 20 μm and 5 μm beads was 29.9 μm at 0.79 sec (90 μm - 60.1 μm), while the experimental result is 27.8 μm . (Figure 5-6) The experimental results are in good agreement with our predictions (see the design calculation in Chapter 3); the difference is 0.3% and 7% respectively.

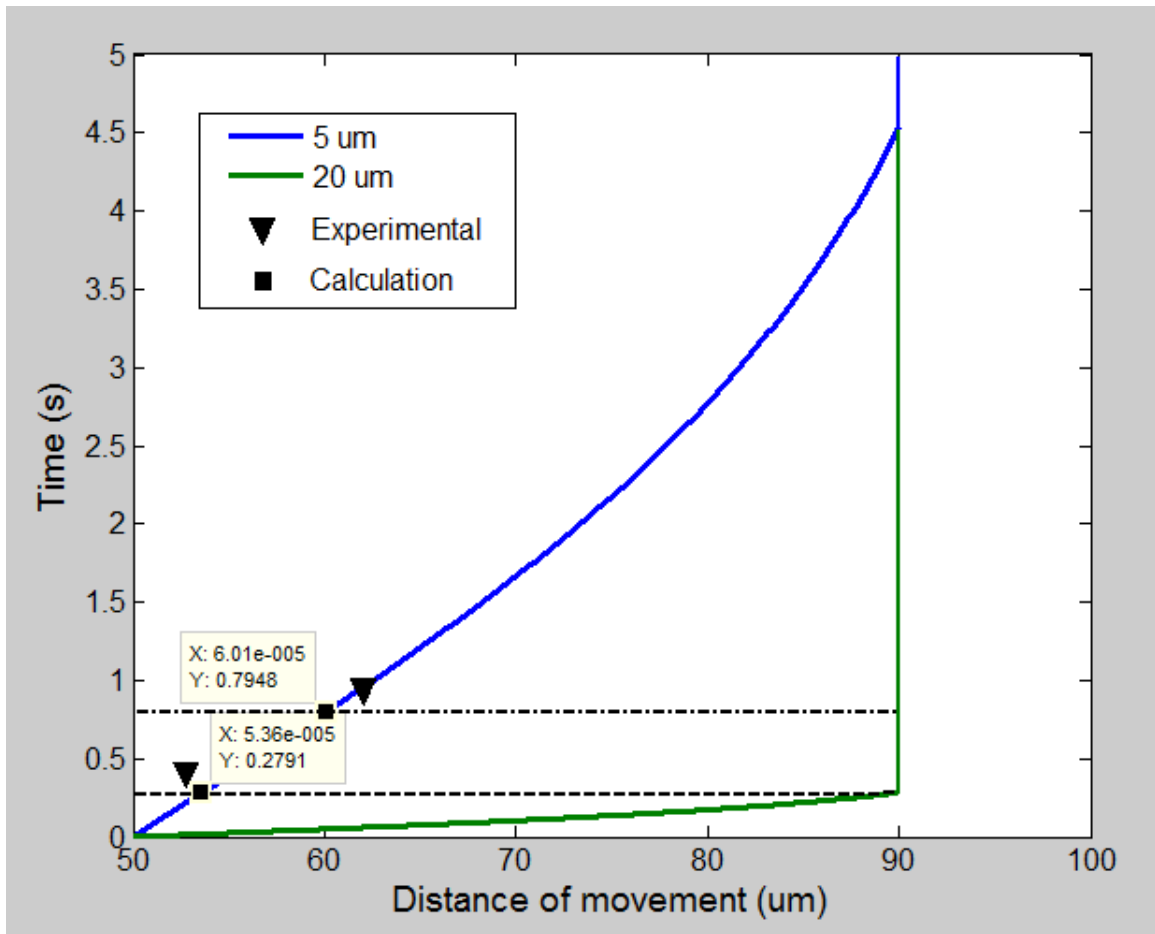


Figure 5-6 Comparison of predicted result from calculation and the experimental result of rectangular box and circle area are showed in Figure 5-5. The distance of two lines reaches the maximum value at the dash line; the dot-dash line shows the distance of two lines in the circle area.

Influences of different voltages applied at the second stage were also studied. A 5 V_{P-P} RF signal (9.48 MHz) was tested. We found it can also separate these two size beads at a flow rate of 25 $\mu\text{L}/\text{hour}$. However, when the flow rate was increased to 50 $\mu\text{L}/\text{hour}$, the separation effect is not obvious at the 2nd stage. In order to get a good separation result at the second stage, the throughput had to be reduced to 25 $\mu\text{L}/\text{hour}$. A RF signal (9.48 MHz) with higher voltage (10 V_{P-P}) was tested as well. However, no obvious observation was observed, because that strong RF signal drove all particles to the pressure node lines at the 2nd stage.

Applied Voltage	Result	Throughput
5 V_{P-P}	Separated	25 $\mu\text{L}/\text{hour}$
7 V_{P-P}	Separated	50 $\mu\text{L}/\text{hour}$
10 V_{P-P}	Not separated	

Table 5-1 Throughput of good separation result with different applied voltage

5.4 Future improvement

Base on the experimental result shown above, different size particles have been separated successfully by using our two-stage SSAW separator. In the next step, we plan to use the particle separator to 1) do blood cell separation, and 2) try to increase the throughput by using wide channel.

5.4.1 Wide channel device

Wider channel allows the SSAW field to form multi-pressure nodes in the channel, which can be considered as multi-channel separation devices. With wide channel device, a much higher throughput can be achieved. We tried to use a wide channel device to separate different size beads, and got some good results in our experiments. But this wide channel device still needs some improvement.

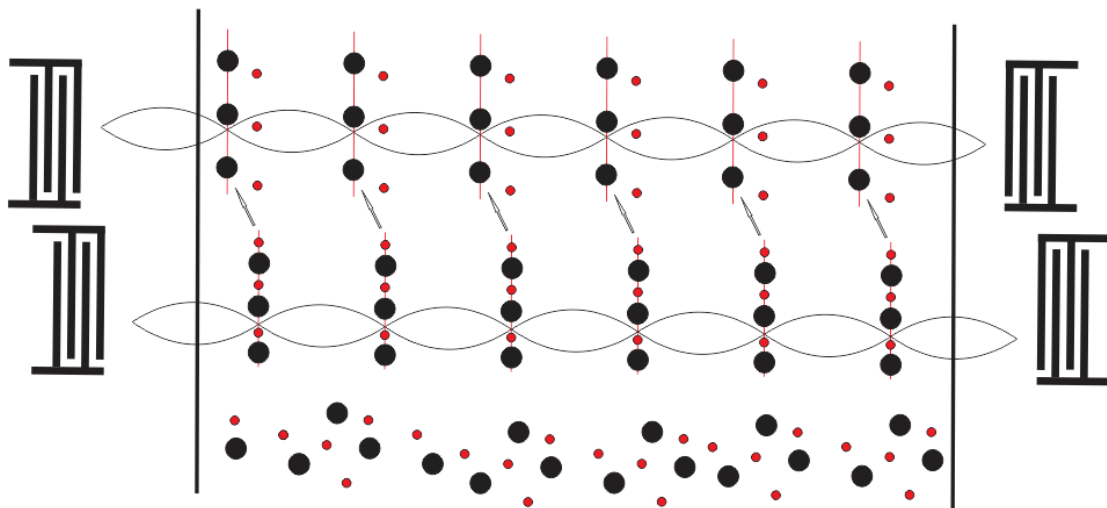


Figure 5-7 Scheme of a wide channel separation device. The channel width was designed as 1200 μm . The design of IDTs is as same as the narrow channel device we presented above.

A wide channel device with a width of 1200 μm was tested. 20 μm polystyrene beads and 7.13 μm polystyrene beads were used in the experiment. At the first stage, by applying 20 $V_{\text{P-P}}$ on the IDTs, all particles were focused in several lines which is the pressure nodes. The applied voltage at the second stage was 6.5 $V_{\text{P-P}}$, then the particles were separated by size. The frequency of

RF signal at both stages was set to 9.48 MHz. The throughput of this separation device can reach up to 300 $\mu\text{L}/\text{hour}$.

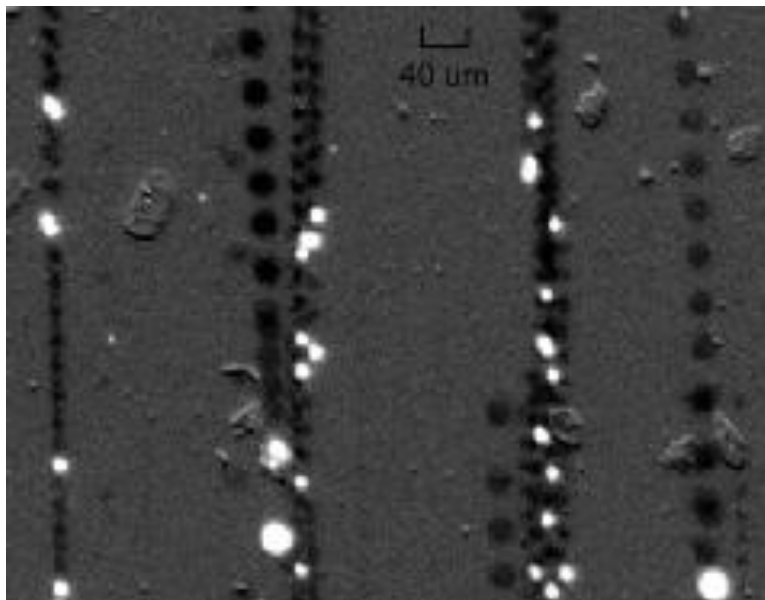


Figure 5-8 Part result of wide channel device. In this picture, beads were first focused into four lines and then separated. This picture is a combination of several pictures shoot by the CCD camera in a short time. The software makes the initial positions of micro particles (the first picture) as white points and positions of micro particles in next few seconds (the rest pictures) as black points, which shows the tendency of particle movement. The voltage applied at the separation stage is 6.5V. Wavelength is 400 μm . The throughput is 300 $\mu\text{L}/\text{hour}$.

The tendency of particle separation in this wide channel device is showed clearly above, which is part of the big channel. Although six pressure nodes (units) were designed at both focusing stage and separation stage, we only got good separation result in four units. (Figure 6-2) The big particles and small

particles were separated successfully at the top area of Figure 6-2; then they can be collected separately with delicate channels at that position.

5.4.2 Feasibility of blood cell separation

Blood cell and plasma separation is critical for many applications, including clinical treatment, DNA analysis, protein identification, antigen verification. The blood separation is a necessary step and foundation of many researches. For example, in clinical application, Red Blood Cell can be used to treat anemia; White Blood Cell can be used to treat agranulocytosis; Platelet can be used to produce platelet-rich plasma, which is very helpful to bone healing; Platelet can also be used to treat hemophilia, which is well known as the link with Queen Victoria; frozen Plasma is a key part in transfusion, which can be seen commonly in the hospital. Blood cell separation relates closely to medical treatment and health care. So blood cell separation is very important and has a bright future.

Next I'll explore the possibility of using SSAW to separate blood cells in diluted blood. Currently blood cell separation is typically done in diluted blood in order to get better separation results. [45, 46] This is because whole blood is with high concentration of blood cells, leading to clog the microchannel easily. Also cell-cell interactions between white blood cell and platelet and among red blood cells can deteriorate the efficiency of separation. In diluted blood, the carrier fluid is diluted plasma, which can be safely modeled as Newtonian fluid. [47] Next, we

will analyze the focusing and separation in diluted plasma. The dimensions of blood cells are much smaller than the wavelength of microwave; the acoustic diffraction will occur; as a result, in our calculation, irregular shape blood cells can be simplified as compressible spheres with a same volume.

Blood mainly consists 4 parts: Red Blood Cell, White Blood Cell, Platelet and Plasma. The parameter for the RBC, WBC, Platelet and Plasma is in the table 5-2.

	Volume (m ³)	Diameter (m)	Density (ρ)(kg/m ³)	Velocity(c) (m/s)	β	Φ(β, ρ)
RBC	9 × 10 ⁻¹⁷	5.56 × 10 ⁻⁶	1115	1600	3.5 × 10 ⁻¹⁰	0.33
WBC	9.05 × 10 ⁻¹⁶	12 × 10 ⁻⁶	1070	1600	3.65 × 10 ⁻¹⁰	0.27
Platelet	1.41 × 10 ⁻¹⁷	3 × 10 ⁻⁶	1060	1600	3.68 × 10 ⁻¹⁰	0.25
Plasma			1025	1450	4.64 × 10 ⁻¹⁰	

Table 5-2 Parameter of blood cells

β and Φ(β, ρ) of the each cell can be calculated with the formula below:

$$\beta = \frac{1}{\rho \cdot c^2}$$

(Where ρ and c are the density of program and the velocity of sound wave transferred in the program, respectively.)

Because of the irregular shape of cells, an approximate volume and calculated the relative radius were used as the parameter.

In order to get a high flow rate, a smaller wavelength is preferred. But the width of channel, which correlates to the wavelength, can not be too small; otherwise the particles may mix with each other. In general, at separating stage, the width of channel should be bigger than 10 times of the diameter of largest blood cell (WBC).

The wavelength (λ) of $300 \mu\text{m}$ was selected to calculation the possibility of the blood separation.

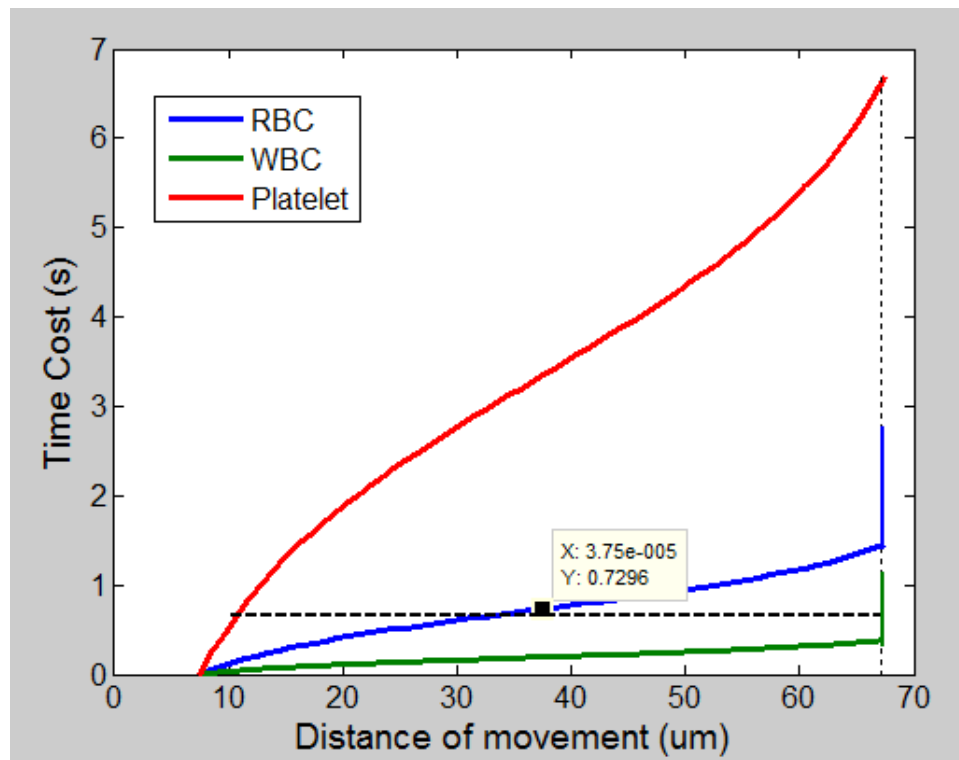


Figure 5-9 Relationship of time and movement of RBC, WBC and Platelet. The dash line shows the distance between three types of blood cells. Dot line shows the time cost of the focusing stage for different blood cells. Wavelength is $300 \mu\text{m}$ and applied voltage is set to be $30 V_{P-P}$.

➤ At focusing stage, working area= $8 \times 10^{-4} \text{ m}^2$, input voltage is 30 V_{P-P} , while input power is 2.25 W. The viscosity of plasma is 1.16×10^{-3}

The initial position and the balanced position, which is near the pressure node of the SSAW, are defined as $x_1 = \frac{\lambda}{40}$, $x_2 = \frac{9\lambda}{40}$, respectively. The needed time t for focusing is calculated with the equations listed in Chapter 3:

$$t_{WBC} = 0.38s, \quad t_{RBC} = 1.45s, \quad t_{pla} = 6.66s$$

➤ At separation stage, in order to make calculation simpler, p_0 can be considered as same as the one we calculated at the focusing stage.

As well, the time cost of the RBC cell moving to the midpoint between pressure node and anti-pressure node is calculated.

$$t_{R40\%} = 0.61s, \quad t_{R50\%} = 0.73s, \quad t_{R60\%} = 0.87s$$

We know that at the same time the WBC has moved to the pressure node ready. Then the movement of the platelet at that time is also obtained.

$$t_{pla15\%} = 0.72s, \quad t_{pla20\%} = 1.32s$$

	WBC	RBC	platelet
Movement of particles at 0.72s (% of wavelength/4)	100%	50%	15%
Distance of movement (μm)	67.5	33.7	10.125

Table 5-3 Calculated movement of different blood cells

So we know that at 0.72s, the WBC is at the pressure node with a movement of 67.5 μm , while the RBC moves about 33.7 μm and the Platelet only

has a movement about 10 μm . As a result, blood cells will be separated successfully and different cells can be collected by using several channels at the end of the second stage.

The bigger input power, the less time cost for both separation and focusing will be needed. The throughput of this separation device can be significantly increased with a higher applied voltage. Use a wide channel can also dramatically increase the flow rate of this separation device.

5.4.3 New substrate material

Integration of SAW particle or droplet manipulation devices with other detection and analysis components into a robust lab-on-a-chip system is very important. LiNbO_3 is a good SAW substrate material and has been widely used in SAW devices, but it is expensive, fragile and cannot be fabricated using micromachining.

Compared to LiNbO_3 , thin film ZnO is cheaper, can be micromachined and permits a higher applied voltage ($> 70\text{V}$). Recent advances in using PDMS micorchannels and ZnO substrate for SAW particle/droplet manipulation has made these devices easy to be fabricated, miniaturized and integrated, and more cost-effective. The resultant lab on a chip system should benefit many applications in biological and medical research.

CHAPTER VI

CONCLUSION

A new micro particle separation device based on standing surface acoustic force was demonstrated in the thesis. This device only utilizes standing surface acoustic force and does not induce sheath flow and dimension changes of the microchannel, thus greatly simplified flow controls and avoided the risk of contamination. This separation device is non-invasive, requires no pretreatment of the particles and work for nearly any type of microscale particles regardless of their optical or charge properties. Surface acoustic force is harmless to biological objects such as blood cells, provided an ideal particle manipulation methods for lab-on-a-chip devices.

With this demonstrated separation device, different size particles, 20 μm polystyrene beads and 5 μm polystyrene beads, were focused in one pressure node line at the first stage by the acoustic forces generated by a strong SSAW field; then the particles were driven to the new pressure node line by a relatively weak SSAW field at the second stage. Because of the larger acoustic force acting on large particles, the bigger particles moved more quickly than the smaller particles, hence these particles with different sizes were separated successfully. The frequency of applied signal was optimized to be 9.48 MHz for

both stages; the applied voltage of first and second stage was set to $20V_{P-P}$ and $7V_{P-P}$, respectively, to get the best separation results. This device worked well with a high throughput of $50 \mu\text{L}/\text{hour}$ compared to the throughput of less-than $20 \mu\text{L}/\text{hour}$ that existing similar devices have.

A similar SSAW separation device with a wide channel was also tested, which can increase the throughput dramatically. The throughput of this wide channel device can reach up to $300 \mu\text{L}/\text{hour}$. From calculation made in Chapter 6, the feasibility of blood separation based on surface acoustic wave was studied and confirmed. Red blood cell, White blood cells and Platelet can be separated in about 0.7 seconds.

REFERENCES

- [1] E. Sollier, H. Rostaing, P. Pouteau, Y. Fouillet, and J. Achard, "Passive microfluidic devices for plasma extraction from whole human blood," *Sensors and Actuators B: Chemical*, vol. 141, no. 2, pp. 617-624, Sep. 2009.
- [2] D. Di Carlo, J. F. Edd, D. Irimia, R. G. Tompkins, and M. Toner, "Equilibrium Separation and Filtration of Particles Using Differential Inertial Focusing," *Analytical Chemistry*, vol. 80, no. 6, pp. 2204-2211, Mar. 2008.
- [3] X. Xuan, J. Zhu, and C. Church, "Particle focusing in microfluidic devices," *Microfluidics and Nanofluidics*, vol. 9, pp. 1-16. 2010.
- [4] M. I. Rocha-Gaso, C. March-Iborra, Á. Montoya-Baides, and A. Arnau-Vives, "Surface Generated Acoustic Wave Biosensors for the Detection of Pathogens: A Review," *Sensors*, vol. 9, no. 7, pp. 5740-5769, 2009.
- [5] R. Singh, S. K. Sankaranarayanan, and V. R. Bhethanabotla, "Enhancement of acoustic streaming induced flow on a focused surface acoustic wave device: Implications for biosensing and microfluidics," *Journal of Applied Physics*, vol. 107, no. 2, p. 024503, 2010.
- [6] T. A. Franke and A. Wixforth, "Microfluidics for miniaturized laboratories on a chip," *ChemPhysChem*, vol. 9, no. 15, pp. 2140-2156, 2008.
- [7] L. Y. Yeo and J. R. Friend, "Ultrafast microfluidics using surface acoustic waves," *Biomicrofluidics*, vol. 3, p. 012002, 2009.
- [8] B. Y. Qu, Z. Y. Wu, F. Fang, Z. M. Bai, D. Z. Yang, and S. K. Xu, "A glass microfluidic chip for continuous blood cell sorting by a magnetic gradient without labeling," *Analytical and Bioanalytical Chemistry*, vol. 392, no. 7, pp. 1317-1324, 2008.

- [9] L. C. Jellema, T. Mey, S. Koster, and E. Verpoorte, "Charge-based particle separation in microfluidic devices using combined hydrodynamic and electrokinetic effects," *Lab on a Chip*, vol. 9, no. 13, pp. 1914–1925, 2009.
- [10] J. C. Baret et al., "Fluorescence-activated droplet sorting (FADS): efficient microfluidic cell sorting based on enzymatic activity," *Lab on a Chip*, vol. 9, no. 13, pp. 1850–1858, 2009.
- [11] T. Braschler, N. Demierre, E. Nascimento, T. Silva, A. G. Oliva, and P. Renaud, "Continuous separation of cells by balanced dielectrophoretic forces at multiple frequencies," *Lab on a Chip*, vol. 8, no. 2, pp. 280–286, 2008.
- [12] M. Abdelgawad, M. W. Watson, and A. R. Wheeler, "Hybrid microfluidics: A digital-to-channel interface for in-line sample processing and chemical separations," *Lab on a Chip*, vol. 9, no. 8, pp. 1046–1051, 2009.
- [13] M. W. Watson, M. M. Jebrail, and A. R. Wheeler, "Multilayer Hybrid Microfluidics: A Digital-to-Channel Interface for Sample Processing and Separations," *Analytical chemistry*, vol. 82, pp. 6680-6686, 2010.
- [14] H. H. Cui, J. Voldman, X. F. He, and K. M. Lim, "Separation of particles by pulsed dielectrophoresis," *Lab on a Chip*, vol. 9, no. 16, pp. 2306–2312, 2009.
- [15] P. Augustsson, J. Persson, S. Ekström, M. Ohlin, and T. Laurell, "Decomplexing biofluids using microchip based acoustophoresis," *Lab on a Chip*, vol. 9, no. 6, pp. 810–818, 2009.
- [16] M. Evander, A. Lenshof, T. Laurell, and J. Nilsson, "Acoustophoresis in Wet-Etched Glass Chips," *Analytical chemistry*, vol. 80, no. 13, pp. 5178–5185, 2008.
- [17] A. Lenshof et al., "Acoustic whole blood plasmapheresis chip for prostate specific antigen microarray diagnostics," *Analytical chemistry*, vol. 81, no. 15, pp. 6030–6037, 2009.

- [18] O. Manneberg, J. Svennebring, H. M. Hertz, and M. Wiklund, "Wedge transducer design for two-dimensional ultrasonic manipulation in a microfluidic chip," *Journal of Micromechanics and Microengineering*, vol. 18, p. 095025, 2008.
- [19] S. S. Guo et al., "Ultrasonic particle trapping in microfluidic devices using soft lithography," *Applied physics letters*, vol. 92, p. 213901, 2008.
- [20] B. Jung, K. Fisher, K. D. Ness, K. A. Rose, and R. P. Mariella Jr, "Acoustic particle filter with adjustable effective pore size for automated sample preparation," *Analytical chemistry*, vol. 80, no. 22, pp. 8447–8452, 2008.
- [21] J. Shi, X. Mao, D. Ahmed, A. Colletti, and T. J. Huang, "Focusing microparticles in a microfluidic channel with standing surface acoustic waves (SSAW)," *Lab on a Chip*, vol. 8, no. 2, p. 221-223, 2008.
- [22] J. Shi, H. Huang, Z. Stratton, Y. Huang, and T. J. Huang, "Continuous particle separation in a microfluidic channel via standing surface acoustic waves (SSAW)," *Lab on a Chip*, vol. 9, no. 23, pp. 3354–3359, 2009.
- [23] J. Shi, D. Ahmed, X. Mao, S. C. Lin, A. Lawit, and T. J. Huang, "Acoustic tweezers: patterning cells and microparticles using standing surface acoustic waves (SSAW)," *Lab on a Chip*, vol. 9, no. 20, pp. 2890–2895, 2009.
- [24] C. D. Wood, S. D. Evans, J. E. Cunningham, R. O'Rourke, C. Wälti, and A. G. Davies, "Alignment of particles in microfluidic systems using standing surface acoustic waves," *Applied Physics Letters*, vol. 92, p. 044104, 2008.
- [25] C. D. Wood et al., "Formation and manipulation of two-dimensional arrays of micron-scale particles in microfluidic systems by surface acoustic waves," *Applied Physics Letters*, vol. 94, p. 054101, 2009.
- [26] T. Franke, A. R. Abate, D. A. Weitz, and A. Wixforth, "Surface acoustic wave (SAW) directed droplet flow in microfluidics for PDMS devices," *Lab on a Chip*, vol. 9, no. 18, pp. 2625–2627, 2009.

- [27] T. Franke, S. Braunmüller, L. Schmid, A. Wixforth, and D. A. Weitz, "Surface acoustic wave actuated cell sorting (SAWACS)," *Lab on a Chip*, vol. 10, no. 6, pp. 789–794, 2010.
- [28] R. Shilton, M. K. Tan, L. Y. Yeo, and J. R. Friend, "Particle concentration and mixing in microdrops driven by focused surface acoustic waves," *Journal of Applied Physics*, vol. 104, no. 1, p. 014910, 2008.
- [29] J. K. Luo et al., "Moving-part-free microfluidic systems for lab-on-a-chip," *Journal of Micromechanics and Microengineering*, vol. 19, p. 054001, 2009.
- [30] A. Renaudin, V. Chabot, E. Grondin, V. Aimez, and P. G. Charette, "Integrated active mixing and biosensing using surface acoustic waves (SAW) and surface plasmon resonance (SPR) on a common substrate," *Lab on a Chip*, vol. 10, no. 1, pp. 111–115, 2010.
- [31] Y. Bourquin, J. Reboud, R. Wilson, and J. M. Cooper, "Tuneable surface acoustic waves for fluid and particle manipulations on disposable chips.," *Lab on a Chip*, vol. 10, no. 15, p. 1898-1901, 2010.
- [32] A. ZHANG, L. YE, and L. FEI, "Research on the Transportation of Digital Micro Fluids Between Two Substrates Based on Surface Acoustic Wave," *CHINESE JOURNAL OF SENSORS AND ACTUATORS*, vol. 22, no. 10, pp. 1382-1386, 2009.
- [33] X. Y. Du, Y. Q. Fu, J. K. Luo, A. J. Flewitt, and W. I. Milne, "Microfluidic pumps employing surface acoustic waves generated in ZnO thin films," *Journal of Applied Physics*, vol. 105, no. 2, p. 024508, 2009.
- [34] M. Cecchini, S. Girardo, D. Pisignano, R. Cingolani, and F. Beltram, "Acoustic-counterflow microfluidics by surface acoustic waves," *Applied Physics Letters*, vol. 92, no. 10, p. 104103, 2008.
- [35] S. Girardo, M. Cecchini, F. Beltram, R. Cingolani, and D. Pisignano, "Polydimethylsiloxane–LiNbO₃ surface acoustic wave micropump devices for fluid control into microchannels," *Lab on a Chip*, vol. 8, no. 9, pp. 1557–1563, 2008.

- [36] L. Masini, M. Cecchini, S. Girardo, R. Cingolani, D. Pisignano, and F. Beltram, "Surface-acoustic-wave counterflow micropumps for on-chip liquid motion control in two-dimensional microchannel arrays," *Lab on a Chip*, vol. 10, no. 15, pp. 1997–2000, 2010.
- [37] L. Y. Yeo and J. R. Friend, "SURFACE ACOUSTIC WAVES: A NEW PARADIGM FOR DRIVING ULTRAFAST BIOMICROFLUIDICS.", *Proceedings of the ASME 2009 2nd Micro/Nanoscale Heat & Mass Transfer International Conference*.
- [38] Y. Q. Fu et al., "Recent developments on ZnO films for acoustic wave based bio-sensing and microfluidic applications: a review," *Sensors and Actuators B: Chemical*, vol. 143, no. 2, pp. 606–619, 2010.
- [39] Guan Zhang and Yigui Li, "Trends of Micro Actuators Based on Surface Acoustic Waves," *Micronanoelectronic Technology*, vol. 9, pp. 540-545, 2009.
- [40] Jeonghun Nam, Yongjin Lee and Sehyun Shin, "Size-dependent microparticles separation through standing surface acoustic waves," *Microfluidics and Nanofluidics*, vol. 11, no. 3, pp. 317-326, 2011.
- [41] James Friend and Leslie Yeo, "Microscale acoustofluidics: Microfluidics driven via acoustics and ultrasonics," *Reviews of Modern Physics*, vol. 83, no. 2, pp. 647-704, 2011.
- [42] Zhuochen Wang and Jiang Zhe, "Recent advances in particle and droplet manipulation for lab-on-a-chip devices based on surface acoustic waves," *Lab on a Chip*, vol. 11, no. 7, pp. 1280-1285, 2011.
- [43] Keji Yang and Baolong Zhang, "Theoretical research on ultrasonic radiation force of micro-components," *Journal of Engineering Design*, vol. 11, no. 6, pp. 316-320, 2004.
- [44] K Yosioka and Y Kawasima, "Acoustic radiation pressure on a compressible sphere," *Acustica*, vol. 5, no. 3, pp. 167-173, 1955.

- [45] Matthew S. Pommer, Yanting Zhang, Nawarathna Keerthi, Dong Chen, James A. Thomson, Carl D. Meinhart, Hyongsok T. Soh, "Dielectrophoretic separation of platelets from diluted whole blood in microfluidic channels," *Electrophoresis* vol. 29, no.6, pp.1213–1218, 2008.
- [46] Han Wei Hou, Ali Asgar S Bhagat, Wong Cheng Lee, Sha Huang, Jongyoon Han, Chwee Teck Lim, "Microfluidic Devices for Blood Fractionation," *Micromachines*, vol.2, no.3, pp.319-343, 2011.
- [47] J Harkness, "The viscosity of human blood plasma; its measurement in health and disease." *Biorheology*, Vol.8, no. 3, pp. 171-193, 1971.

APPENDICIES

APPENDIX A:
TABLE OF EQUIPMENT

Equipment	Company	Type
Amplifier	OPHIR-RF	5302032
DC power	RL-US	PS1-150W-28
DCC camera	Q-IMAGING	QI CAM
Function generator	33522A	Agilent
Hot plate	Barnstead Int.	HP131225
Microscope	Mitutoyo	FS70
Oscillograph	Agilent	DSO 6054A
Plasma cleaner	Harrick plasma	PDC-32G
Profilometer	Veeco	Dektak 150
Spin-coater	Laurell	WS-400B-6NPP/LITE
Syringe pump	KD Scientific	KDS-100
Ultrasonic sink	Branson	3510
UV mask aligner	OAI	206
Wafer cutter	Sherline	5410

APPENDIX B:
TABLE OF EXPERIMENTAL MATERIALS

Material	Company	Type
5 μm particles	Fluka	79633-10ML-F
20 μm particles	Fluka	74491-5ML-F
Alcohol	Pharmco-Aaper	Ethyl Alcohol
AZ4620	AZ	P4620
AZ developer	AZ	AZ 400K
AZ striper	AZ	AZ 400T
Cr etchant	Transene Co., Inc	Chromium etchant 1020
Glass Substrate	VWR	Micro slides 25*75
IPA	Macrom	Isopropyl Alcohol
LiNbO_3	Roditi Int. Corp. Ltd.	LN 4" 128 deg Y-cut wafer
PDMS	Sylgard	184 silicone elastomer kit
SU8	Micro Chem	SU-8 2075
SU8 developer	Micro Chem	SU-8 developer
Surfactant	Fisher Biotech	Triton-X-100